Development of Wavelength-shifting Fibers with high Photon Capture-Rate

Bastian Keßler

10.01.2024

FB08
Institute of Physics
AG Böser

Documentation

Development of Wavelength-shifting Fibers with high Photon Capture-Rate

Bastian Keßler

1. Reviewer Prof. Dr. Sebastian Böser
Institute of Physics - Etap
Johannes Gutenberg University Mainz

2. Reviewer Prof. Dr. Alfons Weber
Institute of Physics - Etap
Johannes Gutenberg University Mainz

Supervisors Sebastian Böser and John Rack-Helleis

10.01.2024

Bastian Keßler
Development of Wavelength-shifting Fibers with high Photon Capture-Rate
Documentation, 10.01.2024
Reviewers: Prof. Dr. Sebastian Böser and Prof. Dr. Alfons Weber
Supervisors: Sebastian Böser and John Rack-Helleis

Johannes Gutenberg University Mainz
AG Böser
Institute of Physics
FB08
Staudingerweg 7
55128 Mainz

Danksagung

Zunächst möchte ich allen danken, die mich auf meinem Weg unterstützt haben. Mein herzlichster Dank gilt meiner Familie, auf deren finanzielle und vor allem seelische Unterstützung ich mich immer verlassen konnte. Ich möchte auch Dr. Anastasia Mpoukouvalas danken, ohne deren Mitwirken das Kapitel über das Clumping nicht möglich gewesen wäre. Und auch Alfons Weber für die Übernahme der Zweitkorrektur.

Kommen wir nun zu meinen Kollegen aus der AG Böser und den paar Abtrünnigen, die sich in unserem Büro niedergelassen haben. Eure Gesellschaft und das gemeinsame Diskutieren der eigenen Probleme haben mich stets motiviert und inspiriert.

Ein besonderer Dank geht an John Rack-Helleis für seine ständige Hilfsbereitschaft und vor allem seine ansteckende Motivation.

Zuletzt möchte ich mich noch bei meinem Betreuer und Professor Sebastian Böser bedanken, für die Möglichkeit, an diesem interessanten und nur manchmal frustrierenden Thema forschen zu dürfen. Es war mir eine Freude, ein Teil Ihrer Arbeitsgruppe gewesen zu sein. Sei es die anregenden und freundlichen Diskussionen, die ich mir zumindest meistens zu Herzen genommen habe aber vorallem Ihr persönlicher Einsatz für die Fertigstellung dieser Arbeit.

Fig. 1.: Created with Bing Image Creator (10.01.24)

Contents

1 Introduction and Motivation

Neutrinos are one of the most elusive and hard to detect particles in the standard model of physics. Their detection requires very large instrumented volumes to compensate for their tiny interaction rate with matter. Neutrino experiments such as IceCube[1] or the upcoming NuDoubt++[2] utilize the Cherenkov effect or scintillation technology to indirectly measure neutrino signatures. The photons generated in this interaction are produced to a large fraction in the UV regime. However, the current state of the art photo sensors with single photon resolution, the photomultiplier tube, is not sensitive to photons in the UV range. It is therefore envisioned to employ wavelength-shifting technologies to enhance the detection capabilities of the neutrino experiments.

Here wavelength-shifting fibers play a special role, since they are not only capable of shifting the light but also capture light over a large area. This is focused on the small fiber ends, which can give increased signal to noise ratio. This makes them particularly interesting for neutrino experiments based on Cherenkov or scintillation techniques. Their capability to capture light primarily depends on the difference in the refractive indices of their material and the surrounding medium, leading to a capture rate below 10% for a PMMA based fiber in water.
In order to increase the performance of the fibers and thus their range of application, this work investigated how the capture rate can be increased.

In commercially available fibers the wavelength shifter molecules are distributed isotropically in the fiber's core. However, from a purely geometrical argument (section 4.1), it is advantageous to situate the wavelength shifter molecules as close to the fiber´s surface as possible. The increased overall capture efficiency has been successfully demonstrated in the WOM project[3] using large diameter hollow tubes and is now applied to small diameter fibers. The theoretically obtainable gain in capture efficiency is a factor of 2 in the case of a quartz fiber with air as surrounding medium. For smaller differences in refractive index between the media, the factor is higher and we obtain a factor of 4 for the case of the same fiber in water.

It was investigated in chapter 5 how the performance parameters timing, TIR capture efficiency and attenuation are affected when the carrier material diameter is reduced

to the order of mm. However, measurements of the attenuation length of the tested fibers yield values of around $2\,\mathrm{m}$, which is smaller than the achieved attenuation length of commercially available fibers with around $3\,\mathrm{m}$. In chapter 6, possible reasons for the lower attenuation length have been investigated in detail. These include intermolecular effects like clumping, shown in section 6.3. Additionally the impact of self-absorption due to the higher relative amount of paint thickness compared to the fiber diameter was examined in subsection 6.4.1. As a theoretical counterpart to the measurements, a detailed numerical model was developed in chapter 7 to describe the attenuation of the new fibers.

2 Theory

This chapter introduces the fundamental physical concepts required to understand the photon interactions with and in wavelength-shifting fibers.

2.1 Total Internal Refraction

The following section is based on [4].

Although a part of the light wave is always reflected at the transition to another medium looking at the Fresnel formula [4], for the production of optical fibers, the guided photons must remain reliably trapped in the fiber. To prevent the photons from leaving the fiber, we use the effect of total internal reflection.

The phenomenon of total internal reflection occurs when light propagates from an optically denser medium to an optically less dense medium. This phenomenon is based on the law of refraction, also known as Snell's Law.

Snell's Law states that the incident angle θ_1 and the refracted angle θ_2 of a light ray passing from one medium to another are related by the equation:

$$n_1 \sin(\theta_1) = n_2 \sin(\theta_2) \tag{2.1}$$

Here, we denote:

- n_1 : refractive index of the first medium (optically denser medium),
- n_2 : refractive index of the second medium (optically less dense medium),
- θ_1 : incident angle of the light ray,
- θ_2 : refracted angle of the light ray.

If the refractive index of the second medium n_2 is smaller than the refractive index of the first medium n_1, it may happen that the refracted angle θ_2 becomes greater than $90°$.

Since the sine of an angle cannot be greater than 1, this implies that there is no refracted angle satisfying the condition. In this case, the light is entirely reflected at the interface between the two media. This effect is called Total Internal Reflection (TIR).

Total internal reflection occurs for every angle θ_1 exceeding the critical angle θ_{crit}.

$$sin(\theta_{crit}) = \frac{n_2}{n_1} \; (sin(\theta_2 = 90°)) \tag{2.2}$$

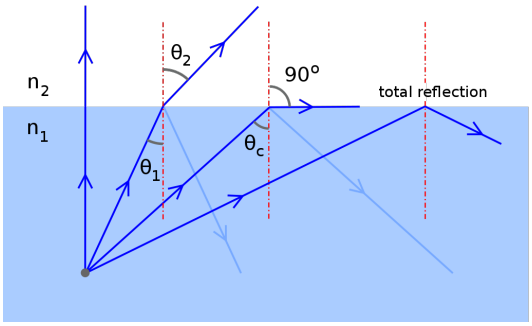

Fig. 2.1.: Refraction of a light beam at an interface between two media with refractive indices n_1 and n_2. Image taken from [@5]

A well-known example of total internal reflection occurs when light transitions from water (optically denser medium) to air (optically less dense medium) with a sufficiently large incident angle. This phenomenon also plays a crucial role in fiber optics, where light rays within a fiber optic cable are guided by total internal reflection.

2.2 Wavelength shifters

The following section is based on [6]:

Wavelength shifters are a specical type of scintillators which absorb photons with a short wavelength and emits them at a longer wavelength. It uses the principle of scintillation, which describes the process where an electron is excited into a higher-energy state by an ionizing particle or a high-energy photon. If the electron falls back to its original energy level, a photon with the energy difference of the two states is re-emitted isotropically. Here a distinction must be made between the case of fluorescence, in which the excited state decays almost instantly (ns range),

and phosphorescence, where the lifetime is significantly longer due to forbidden energy states. So scintillators that are excited by light (photoluminescence) and whose re-emission is via fluorescence are generally referred as wavelength shifters. For this work we consider the scintillation mechanism for organic wavelength shifter molecules. The energy bands of organic wavelength shifters result from so-called π electrons which are generated by the overlapping of p orbitals (e.g. double C=C bonding). An example of the resulting energy levels can be found in Fig. 2.2. S_0 and S_1 represent singlet states which are further subdivided into various thermal excitation's S_{1N}.

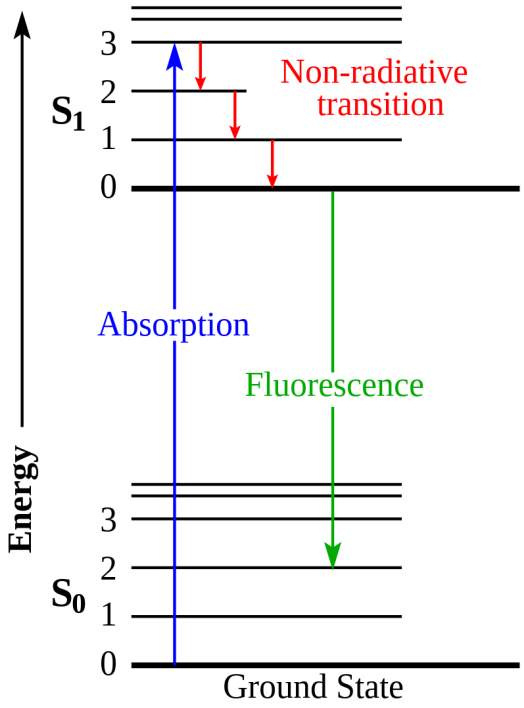

Fig. 2.2.: Energy levels of an organic wavelength-shifting molecule. The reemitted photon from the fluorescence has a lower energy than the absorbed photon, due to the additional non radiative losses.[@7]

For fluorescence, an electron is excited from its ground state S_{00} to an excited state S_{1x} by absorbing a photon. To get back to the ground state the electron has to loose the gained energy. In order to loose energy it has two "possibilities". The first possibility is the re-emission of a photon with the energy difference between the states and the second a non-radiative transition where it transfers some of its energy to the environment as thermal energy. Since the exited states with thermal energy in molecule vibrations (such as S_{0N} or S_{1N} ; $N > 1$) are not in a thermal equilibrium with the other molecules, their lifetime is relatively short, transferring the thermal energy to the surrounding material. Therefore most of the exited states are in S_{10} before they fall back to one of the vibrational exited ground states S_{0N} by

isotropically emitting a photon Fig. 2.2. After emitting the photon the remaining energy difference to the ground state is released as thermal energy. Since the photons are emitted before reaching the ground state their energy isn't sufficient to excite an electron from the ground state. Because the emitted photons have a lower energy, than the energy difference between ground state and excited state, the photons can leave the molecule without being absorbed. However, a small fraction of photons have energies which are high enough to be absorbed again, this effect is called self-absorption (see Fig. 2.3).

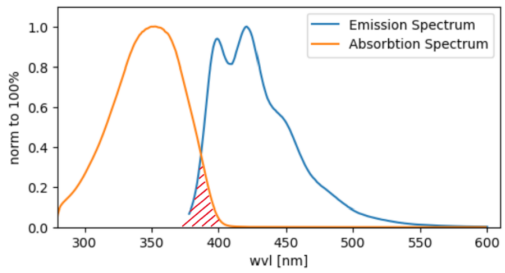

Fig. 2.3.: Absorption (orange) and emission sepctrum (blue) of the wavelength shifter Bis-MSB. The overlap between the spectra where self-absorption occurs is shown in shaded red.

The ratio of emitted to absorbed photons is given by the fluoresence quantum yield Qy and is given by Eq. 2.3.

$$Qy = \frac{\#\text{ of emitted Photons}}{\#\text{ of absorped Photons}} \tag{2.3}$$

The lifetime τ that passes until the photon is re-emitted is made up of the mean life times τ_n of the states passed through until re-emission.

$$\frac{1}{\tau} = \sum_i \frac{1}{\tau_i} \tag{2.4}$$

The number of excited states $N(t)$ after the time t when starting with a number of N_0 excited states can be described by the decay law:

$$N(t) = N_0 \cdot exp\left(-\frac{t}{\tau}\right). \tag{2.5}$$

3 Wavelength-shifting Fiber

In this chapter, the functionality and application of wavelength-shifting fibers is described. In this context, a close look is taken at the relevant performance parameters and the possibility for improvement of those.

3.1 Wavelength-shifting Fibers

Wavelength-shifting fibers (short WLS fibers) are a special type of optical fibers. For standard optical fibers depicted in Fig. 3.1a, light only couples into the fiber at the end faces to satisfy the total internal reflection (TIR) condition Eq. 2.2 while photons incident on the lateral surface are not captured. If however the fiber material contains wavelength shifter molecules, a major fraction of incident light can be absorbed by the wavelength shifter and is consecutively re-emitted isotropically. The fraction of re-emitted photons which now falls under the TIR condition gets trapped inside the fiber and guided to its end faces (see Fig. 3.1b), allowing the fiber to act as a passive light collector.

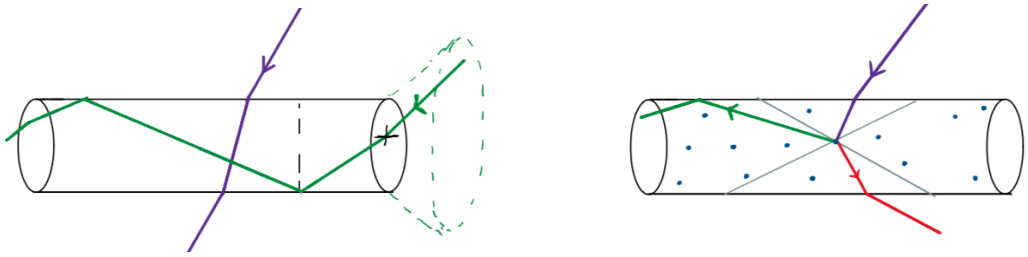

(a) schematic of an optical fiber

(b) schematic of an optical fiber with wavelength-shifting molecules (blue dots)

Fig. 3.1.: Difference between an optical fiber a) and a WLS fiber b). When photons in the UV-range (violet line) laterally hit the fiber, the optical fiber does not capture it. In the case of a WLS fiber, UV photons will be absorbed by the wavelength shifter molecules in the material and re-emitted isotropically. All photons emitted within the cone spanned by the critical angle (green) will be captured within the WLS fiber due to total internal reflection.

The spectrum of captured and emitted light of such fibers depends on the wavelength shifter in use.

It is also possible to combine several shifters to widen the absorption spectrum. In this case a "lower" shifter absorbs and shifts lower wavelengths into the absorption spectrum of an upper shifter, which shifts the light even further. In this way, the fiber is sensitive to the absorption spectra of both wavelength shifters. The emission spectrum of such fibers is then defined by the wavelength shifter working at the longest wavelengths(see Fig. 3.2).

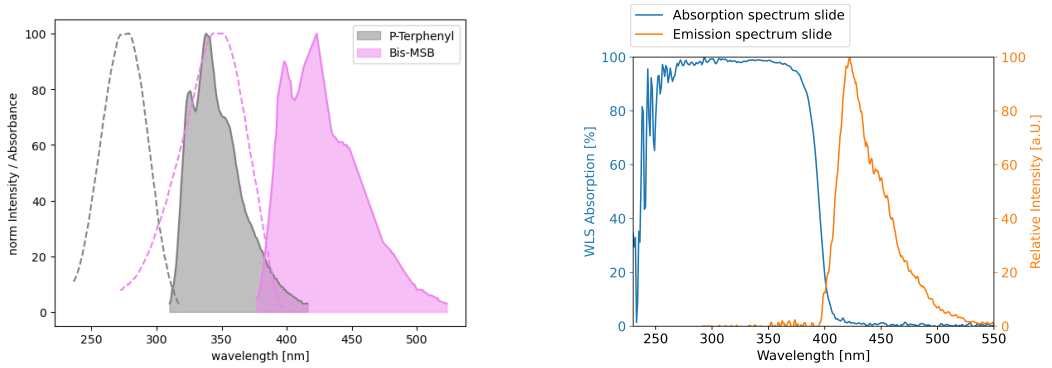

(a) (b)

Fig. 3.2.: Example of two wavelength shifters (Emission spectrum of P-terphenyl in grey and Bis-MSB in purple in Fig. 3.2a. Absorption spectra shown as dashed lines.) used for the Wavelength-shifting Optical Module[3]. Here, P-terpyenyl is the lower shifter, absorbing between $200\,\mathrm{nm}$ to $300\,\mathrm{nm}$. The absorption spectrum of Bis-MSB has a large overlap with the emission spectrum of P-terphenyl. Most photons absorbed by P-terphenyl will therefore be absorbed by Bis-MSB and shifted into the emission spectrum of Bis-MSB. The resulting combined absorption spectrum of both shifter spans over the absorption range of both wavelength shifters. The absorption spectrum for very high concentrations of both wavelength shifters is shown in Fig. 3.2b.

3.2 Applications for WLS Fibers

While standard optical fibers are widely used to transport light from one point to another (e.g. telecommunication applications), the incorporation of wavelength-shifting molecules transforms the fiber into a light collecting device.

The fiber can then be used as a photosensitive area where the light is collected over a large area and guided along the fiber towards a photo sensor detecting the light. This yields a number of advantages: When the detection area is separated from the sensor, the sensor can be placed outside the detector volume. This has the advantage, that the sensors don't occupy usable detector volume. It is also advantageous if the sensors cannot withstand the given environmental conditions e.g. in the beam of a

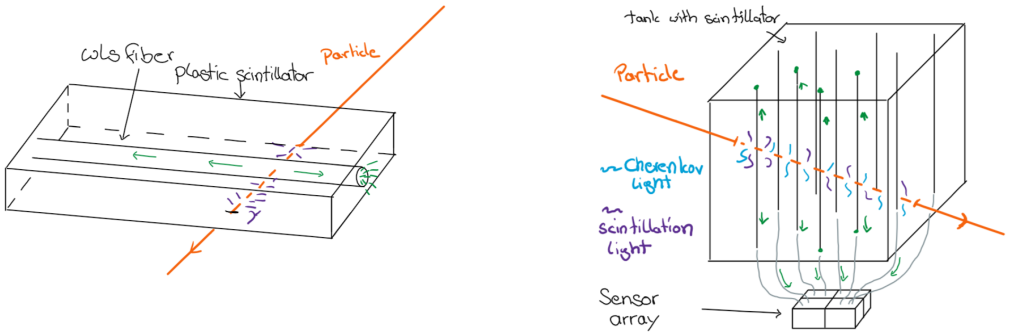

(a) (b)

Fig. 3.3.: Exemplary use cases of WLS fibers. In Fig. 3.3a, a WLS fiber is embedded into a plastic scintillator. When a charged particle propagates through the scintillator, it generates light. This light can then be absorbed by the WLS fiber and is then guided to a detector for readout. This design can also be used as a trigger or veto [8]. In Fig. 3.3b hand side the function of the fibers is similar to that of a wire detector. The fibers collect the light produced by the scintillator or by Cherenkov radiation in a large volume onto a small sensor area [2].

particle accelerator. Moreover the radioactive noise is essentially fixed by the read-out sensors, while a much larger volume can be instrumented allowing an increased Signal-to-Noise Ratio (SNR). The sensors are also more easily to be accessed and to maintain. Last but not least, it is also possible to connect multiple fibers to one sensor, increasing the signal to noise ratio. This can also be used to observe a bigger volume while keeping the number of required (mostly expensive) senors low.

An example of such a detector volume is a combination of WLS fibers with scintillators conceptually presented in Fig. 3.3b. Here, the scintillators generate photons when ionizing particles travel through them. The WLS fibers, embedded in the scintillator volume, collect the photons and guide them to sensor arrays, where they are read out.

Because commonly used wavelength shifters have a decay time in the order of a few ns, this concept can be used as trigger and veto for detectors. The basic concept is shown in Fig. 3.3a. Here a single WLS-fiber is embedded into a plastic scintillator. When ionizing particles travel through the scinitillator, again photons are produced which are collected by the WLS-fiber. The collected light is, once again, guided to the read-out electronics via total internal reflection.

3.3 Performance Parameters

For a WLS fiber we look into three important parameters which can be used to describe its performance:

- Timing: Describes the photon arrival time distribution at a fibers end faces.
- Capture rate: Describes the ratio of photons captured in the WLS-fiber compared to the total number of absorbed photons.
- Attenuation: Describes the light losses for photons traveling inside the fiber as a function of the direct distance between light injection point and end face of the fiber.

3.3.1 Timing

The isolated photon arrival time distribution of a fiber is a convolution of the wavelength-shift timing, following an exponential decay, and the propagation time given by the travel distances of photons inside the tube. The time t_{prop} a photon needs to propagate a distance z along the fiber depends on the velocity along the fiber v_z. Which depends on the refractive index of the fiber medium n_{fiber} and the angle θ to the fiber direction Eq. 3.1.

The time a photon at an angle θ needs to travel a distance d along the fiber is described in Eq. 3.1

$$t_{prop}(\theta) = \frac{n_{fiber}\ d}{c_{vac}\ cos(\theta)}\ ;\ for:\ \theta < \theta_{crit}. \tag{3.1}$$

Here, c_{vac} is the speed of light in the vacuum.

3.3.2 Attenuation

Attenuation describes the reduction of the initial capture intensity I_0 along a distance x. The attenuation itself is described by the attenuation length λ with the equation:

$$I(x) = I_0\ exp\left(-\frac{x}{\lambda}\right) \tag{3.2}$$

The attenuation in the fiber is a combination of absorption and scattering and can be described by their related absorption length λ_{abs} and scattering length $\lambda_{scatter}$, describing the mean free path before the photon gets absorbed or scattered. In case of absorption the photon is lost, while during scattering the photon direction is changed. If the new photon direction satisfies the TIR condition it remains captured inside the fiber, otherwise it is lost. For a WLS fiber, we can therefore treat scattering as a special case of absorption, in which the attenuation caused by scattering is described by the scattering length, divided by the probability p_{loss} that a photon is lost Eq. 3.3. This probability depends on the capture rate and the change of the photon direction. Since the capture rate and the type of scattering don´t change for the same combination of materials, the ratio of the scattering to the absorption remains constant. This means that it is also completely sufficient to consider only the attenuation and its attenuation lengthλ.
The factor that scattering also changes the effective distance is neglected, because in order to play a role the scattering length must be much lower than the absorption length to give a significant increase in the distance, but in that case the whole attenuation would be scattering dominated and the absorption would be irrelevant.

$$I(x) = I_0 \left[exp\left(-\frac{x}{\lambda_{abs}}\right) \cdot exp\left(-\frac{p_{loss}\ x}{\lambda_{scatter}}\right)\right] \tag{3.3}$$

$$= I_0 \cdot exp\left(-\frac{x}{\lambda}\right) \tag{3.4}$$

$$\Rightarrow \frac{1}{\lambda} = \frac{1}{\lambda_{abs}} + \frac{p_{loss}}{\lambda_{scatter}} \tag{3.5}$$

The attenuation length itself depends on the wavelength (wvl) of the light and the material, so for a combination or a mixture of different materials with attenuation lengths λ_n, the total attenuation length depends on the fraction a_n of the distance x that the photon spends in each of them.

$$\frac{1}{\lambda_{total}} = \sum_n \frac{a_n}{\lambda_n} \quad with \sum_n a_n = 1 \tag{3.6}$$

A commercial vendor of fibers, Kuraray, specifies the attenuation length along the fiber[1] of their WLS fibers to lie between $2\,\mathrm{m}$ to $4\,\mathrm{m}$ [@9].

[1]The attenuation length along the fiber is not the same as the attenuation length in the fiber due to different path lengths of the photons subsection 5.2.1

3.3.3 Capture-Rate

The capture rate ϵ_{cap} describes the probability for an absorbed photon to be captured under the TIR condition inside the fiber: To be captured the absorbed photon first has to be reemitted after being absorbed. The probability is called the quantum yield Qy and depends on the wavelength shifter. After being reemitted isotropically the photon has to fall under the TIR condition, the ratioϵ_{TIR} of the emitted photons that fall under the TIR is therefore given by Eq. 3.7 and is called the geometric capture rate. Since the Qy of the wavelength shifters used in this thesis are in the range of .96(Bis-MSB) up to 1(P-terphenyl), we consider the capture rate being equal to the geometric capture rate.

$$\epsilon_{cap} = Qy \cdot \epsilon_{TIR} \tag{3.7}$$

$$\tag{3.8}$$

$$Qy = \frac{reemitted}{absorbed} \; ; \; \epsilon_{TIR} = \frac{captured}{reemitted} \tag{3.9}$$

ϵ_{TIR} only depends on the critical angle θ_{crit} and thus on the difference in the refractive indices of the surrounding medium and the bulk material as described by Eq. 2.2
Considering a bulk material with a refractive index of 1.5 (comparable to PMMA) we get for ϵ_{TIR} 33% [2], and for the case of a combination of a polystyrene(n=1.6) core and a PMMA(1.5) cladding, which is commonly used for cladded WLS-fibers [@9] ϵ_{TIR} is around 7% loosing 93% of the photons before including attenuation.

For the use of a trigger, this may not be a problem, because here the amount of light is often sufficiently high. But if the fibers are used to determine the energy of an event, the energy resolution depends on the amount of detected light. Especially for low energy events where the difference between events results only in a few photons, this low capture rate is a problem.

[2] using Eq. 2.2 for the emission in the center Fig. 4.6

The light that arrives at one end face where it can be measured has to overcome a distance z to the end of the fiber. The portion of the absorbed light that arrives at one side of the fiber is called the one sided efficiency ε_{one}. So for the simplest case where the photons travel directly to the end face, ε_{one} can be described with the attenuation length λ of the material using Eq. 3.2 resulting in Eq. 3.11.

$$\varepsilon_{one}(z) = \frac{photons\ arriving\ at\ one\ end(z)}{absorbed} \tag{3.10}$$

$$\varepsilon_{one} = \frac{1}{2}\epsilon_{cap} \cdot exp\left(-\frac{z}{\lambda}\right) \tag{3.11}$$

4 The Wavelength-shifting Optical Module and the Capture-Rate

The Wavelength-shifting Optical Module (WOM) was developed in the context of the upgrade of the IceCube detector [10]. The functionality of the WOM and the insights obtained during development with regard to the capture rate are explored in this chapter.

Fig. 4.1.: Image of an inner tube of the WOM illuminated by an UV lamp

4.0.1 WOM Design

The WOM Fig. 4.2 is designed to be used in the IceCube Neutrino Observatory at the south pole to measure Cherenkov light from charged secondary particles of neutrino interaction with ice.
To measure this light, a WLS fiber is used that absorbs photons in the wavelength range between $250\,\mathrm{nm}$ to $400\,\mathrm{nm}$. The shifted light is then guided along the fibers to optical sensors.
In the WOM, flat Photomultiplier tubes (PMTs) are used for this purpose. As a main photo sensitive area of the WOM, a quartz tube coated with WLS paint, the so-called inner tube or WOM-Tube Fig. 4.1, is used. The paint is applied to the outside of the tube by dip-coating. Here, the tube is submerged in the paint and pulled out again applying the paint on the outside of the tube. The solvent in the paint, toluene, evaporates during the subsequent drying process, leaving a plastic matrix with embedded wavelength shifters on the outer surface of the tube. section 6.2 This is a difference to conventional fibers, where the wavelength shifter molecules are

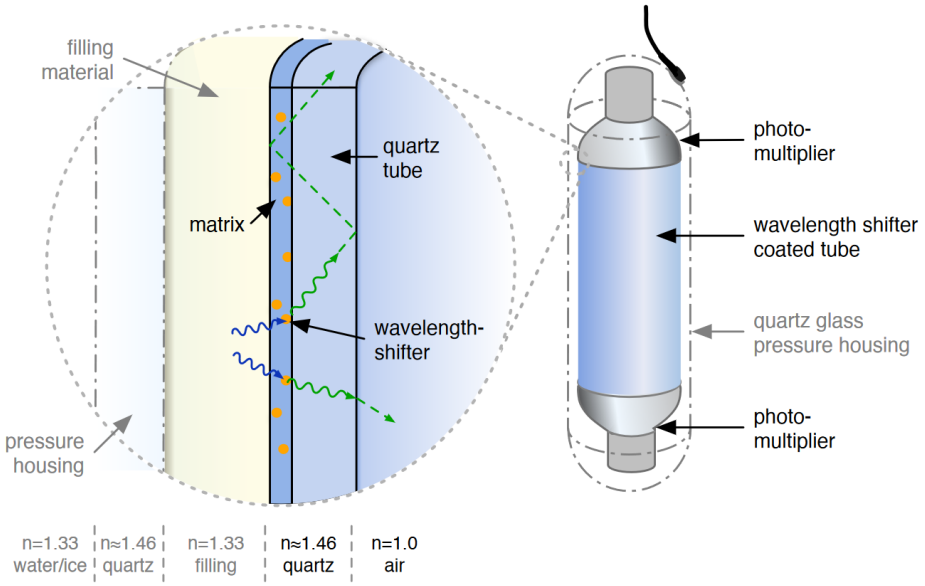

Fig. 4.2.: A schematic drawing of the WOM. UV photons are absorbed in the WLS paint layer and are re-emitted as optical photons. If the emission angle of the photons is larger than the critical angle, they are trapped by total internal reflection and are guided along the tube to PMTs. Image and text from [3]

homogeneously distributed in the fiber material.
Therefore it was investigated whether this offset has an influence on the capture rate of the inner tube.

4.1 Capture-Rate

In order to understand the impact of the absorption and emission point on the capture rate we have to investigate how the angle Φ between the photon path $\vec{\gamma}$ and the normal vector $\vec{n}$ of the surface changes for different emission points.
In order to be captured, a photon has to fulfill the TIR condition:

$$sin(\Phi) \geq \frac{n_{Medium}}{n_{Fiber}} \; ; \; \Phi = \measuredangle(\vec{\gamma}, \vec{n}) \tag{4.1}$$

Since the surface normals do not depend on the point of emission of the photons, we have to look into how the direction of the photons hitting the surface depends on the point of emission. First we look at the general case of a set $\vec{n}$ and an arbitrary photon direction $\vec{\gamma}$ in spherical coordinates. With the fiber direction set along the z axis, therefore normal vector are in the x,y plane. φ is the angle between the photon direction and $\vec{n}$ in the x,y plane and ϑ describes the angle to the z axis Fig. 4.3.

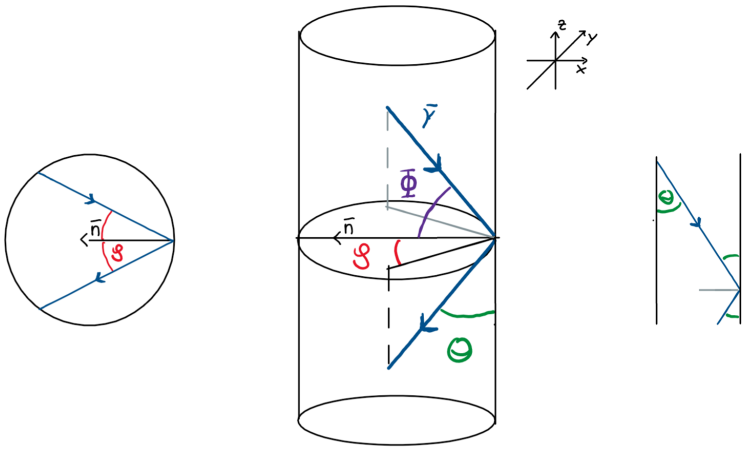

Fig. 4.3.: Choice of the polar coordinates to describe the angle Φ between the photon path and the surface normal $\vec{n}$. φ describes the angle to $\vec{n}$ in the cross section plane(left) and θ the angle to the fiber direction (-z).

So for the $\vec{n}$ chosen in Fig. 4.3 we can calculate Φ:

$$cos(\Phi) = \vec{\gamma} \cdot \vec{n} = \begin{pmatrix} cos(\varphi)sin(\theta) \\ -sin(\varphi)\sin(\theta) \\ -cos(\theta) \end{pmatrix} \cdot \begin{pmatrix} -1 \\ 0 \\ 0 \end{pmatrix} = -cos(\varphi)sin(\theta) \tag{4.2}$$

$$sin(\Phi) = \sqrt{1 - cos^2(\Phi)} \tag{4.3}$$

so in order to fulfill Eq. 4.1:

$$\sqrt{1 - cos^2(\varphi)sin^2(\theta)} \geq \frac{n_{Medium}}{n_{Fiber}} \tag{4.4}$$

Now we look at the impact of the emission point on the distribution of φ and θ. Due to the geometry of the cylinder, the distribution for θ is independent of the position in the cross section plane. Therefor the cone that is spanned by $\theta = arcos\left(\frac{n1}{n2}\right)$ gives a minimum value for the capture rate Fig. 4.6.

For the distribution of φ we look into the plane cross section of the fiber Fig. 4.4a. One can immediately see, that if we start at the center of the fiber all photons will hit the surface vertically and therefore will not contribute to the TIR. If we increase the relative emission radius $x_0 = |\vec{r}|/R$ of a fiber with an outer radius of R and the offset of the emission point $|\vec{r}|$, the photons starts hitting the surface under an angle Fig. 4.4a. The distribution of angles can be described by the radius of the emission ring and the angle α. Looking at Fig. 4.4b φ overall increases with

Fig. 4.4.

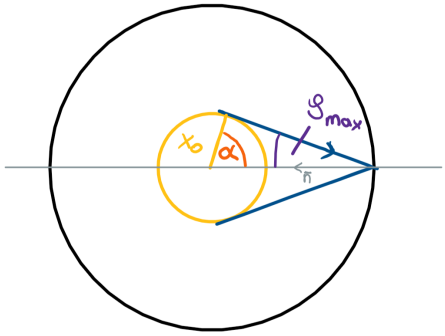

(a) Consideration of photon propagation in the plane and the angle φ as a function of the relative emission radius x_0. For larger raddi, the maximum possible angle for φ also increases

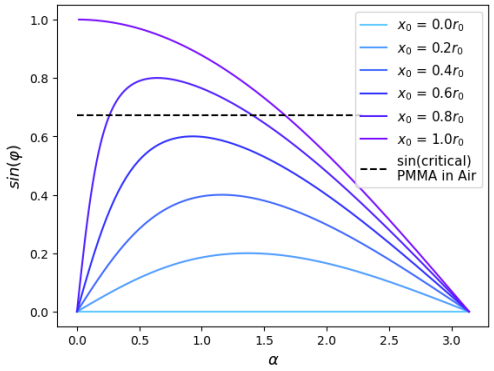

(b) sin φ dependency on the relative emission radius x_0. The closer the emission point is to the surface the overall angle of φ and therefore Φ increases. Eventually getting big enough to fulfill the TIR condition on its own

increasing radii. Therefore more photons fall under the TIR condition Eq. 4.2. Integrating over all photon directions which hit the surface we get the capture rate ϵ_{TIR}. Two examples are shown in Fig. 4.5. For the case of a quartz fiber with refractive index of n = 1.47[@11] in air(n = 1) the capture rate increases by a factor of two just by moving the emission point to the edge. For smaller differences in refractive indices like quartz- (ice , scintillator) the increase is even bigger.

It is therefore possible to increase the capture rate if more photons are absorbed close to the edge. If we also take the refractive indices into account, we notice that the capture rate decreases for a smaller difference in the indices. The efficiency increase obtained when the wavelength shifters are at the surface rather than the middle is higher for smaller differences in the refractive index between the WOM-Tube and the surrounding medium Fig. 4.5. This makes this effect particularly interesting for situations where the difference is small, be it that the fibers are in water, ice or even in a scintillator.

4.2 Performance Parameter

Since the WOM-Tube is similar in function to a WLS fiber and operates with the outer coating, the parameters determined are suitable as a point of reference for the subsequent fibers.
For the performance of the WOM-Tubes, the capture rate, attenuation over the light guide length and the timing are important. All these parameters were determined in

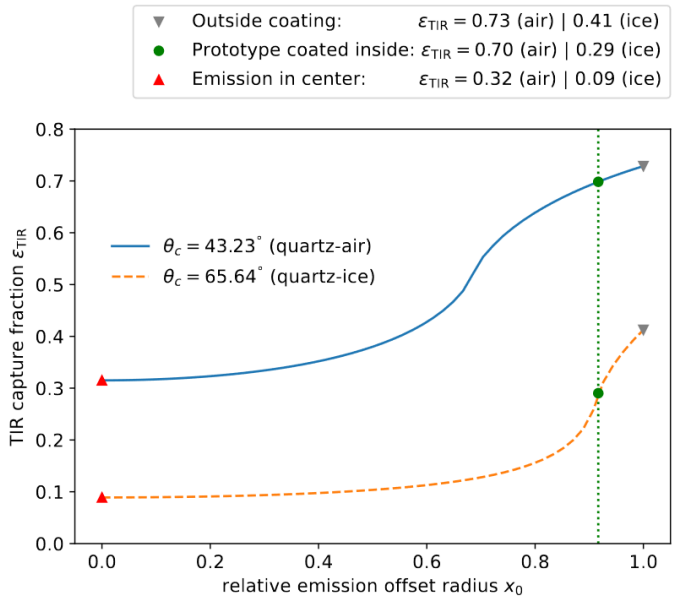

Fig. 4.5.: Fraction ϵ_{TIR} of the solid angle under which emitted photons are captured by total internal reflection as a function of the emission radius x_0 of the emission point. The two lines represent a module immersed in air (solid) or water (dashed). The green dots indicate the capture efficiency for the prototype module, which is coated on the inside of tube. Minimal values for the emission point in the center of the tube and maximal values for emission on the outside of the tube are indicated by triangles. Image and text from [3]

the course of development. The timing is in the 10ns rangeFig. 4.7a, the attenuation length of the inner tube is 3-5 metres and the catch rate is 80% of the maximum achievable Fig. 4.7b. It has therefore already been shown on the basis of the WOM that the predicted increase in the capture rate can be achieved.

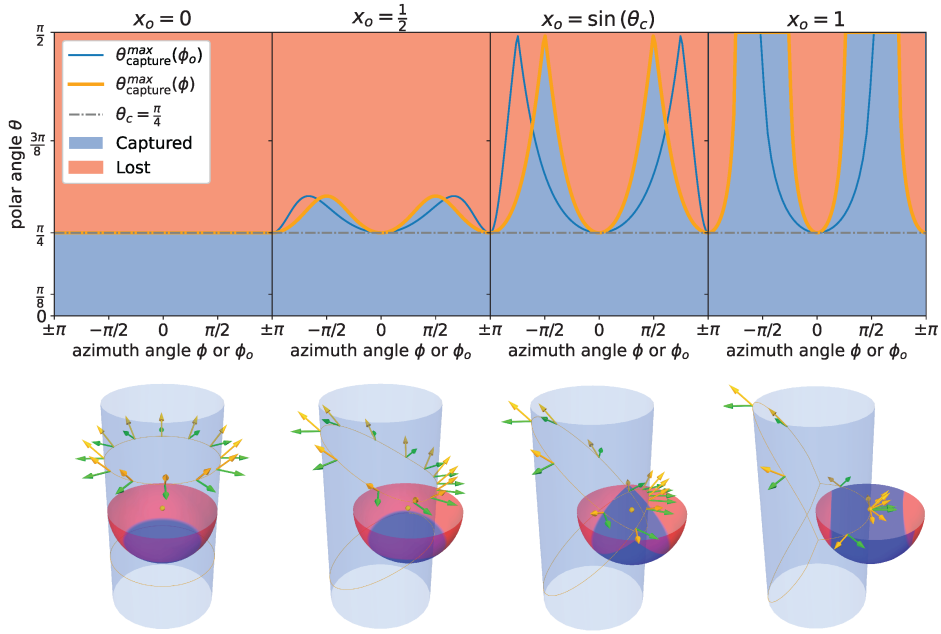

Fig. 4.6.: Illustration of the solid angle under which the photons are captured as a function of the relative fraction of the radius $x_0 = |\vec{r}|/R$ at which the photons are emitted (indicated by the yellow dot). The orange (blue) line in the upper plot indicates photons that encounter the surface under the critical angle as a function of the azimuth angle $\phi(\phi_0)$ relative to the emission point (center of the cylinder). In the upper and middle plots the blue shaded areas indicate solid angle regions under which photon trajectories captured by total internal reflection while red shaded areas show those that are not captured. In the middle plot yellow arrows indicate directions of incident photons, while green arrows depict surface normals. In this example, the critical angle is chosen as $\theta_c = \pi/4$. Image and text from [3]

Fig. 4.7.

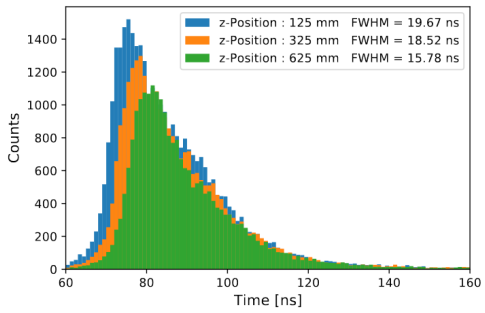

(a) The measured transit time spread of a WOM-Tube with one attached PMT is shown for different for different illumination distances (z-position) to the PMT along the tube. Image and text from [3]

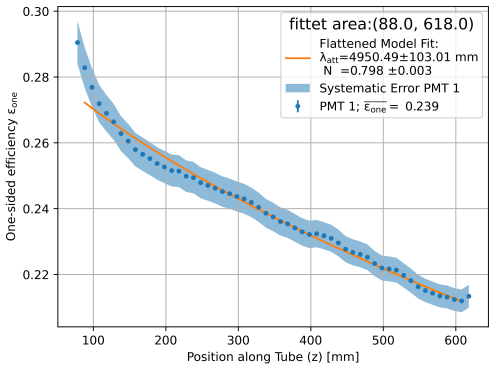

(b) One-sided efficiency ε_{one} of a WOMs inner tube for different z-positions. (In the fitted model the N value represents the portion of the maximum capture rate and λ_{att} is the attenuation length in the tube Eq. 5.3) [Measurement and plot done by John Rack-Helleis]

Development of optimized Fibers

5

This chapter examines the possibility of applying the efficiency increase gained from bringing the wavelength-shifting molecules to the outer surface to build optimized wavelength-shifting fibers (oWl fibers). To achieve this, we use the WOM-Tube and its manufacturing methods as described in detail in [3] as a starting point. The coating substrate are quartz rods in the $1\,\mathrm{mm}$ diameter range. In the following, we examine the impact of the reduction in diameter from WOM-Tube to oWl-fiber on the previously explained performance parameters

Fig. 5.1.: Image of the first test oWl fibers

5.1 Parameters

5.1.1 Capture-Rate

As is known from Fig. 4.5, the capture rate for outer coating depends on the relative distance to the fiber center x_0. So a decrease of the radius of the carrier material for a constant paint thickness will reduce the relative distance of the wavelength shifters to the center.
The paint thickness used for the WOM-Tube is $15\,\mu\mathrm{m}$ to $40\,\mu\mathrm{m}$ while the quartz tube has a radius of $57.5\,\mathrm{mm}$. The emission point is therefore at $x_0 = 0.999$. If the same paint thickness is used for a fiber with a radius of $1\,\mathrm{mm}$ however, we obtain $x_0 = 0.96$. Looking at Fig. 4.5 this may have a small impact for the case of quartz and ice but overall the capture rate is still at a high level. For fibers smaller than $1\,\mathrm{mm}$

the paint thickness has to be reduced in order to keep the increase in capture rate. But a reduction in the thickness of the paint layer will also lead in to a less absorbent paint layer reducing the quantum yield, and with it the overall fiber capture rate.

5.1.2 Timing

As known from subsection 3.3.1, the timing depends largely on two factors: First, the decay times of the wavelength shifters in use. And second the distribution of the path lengths of the photons traveling inside the light guide. Since the same paint mixture is used for the WOM-Tube as for the oWl-fiber, nothing changes for the timing of the wavelength shifter. For the distribution of the photons in θ, the possible photon directions are defined by x_0. But even for the case of $x_0 = 0.96$ the distribution changes only slightly, as was discussed in Fig. 4.6.
The overall timing is therefore nearly identical when transforming from the WOM-Tubes to small fibers.

5.1.3 Attenuation

The attenuation of the photons depends on the medium through which they travel (see subsection 3.3.2). In the WOM/oWl fiber case it is possible, that carrier material and the WLS-paint can have different attenuation lengths.
As the carrier diameter is reduced, the distance spent in the carrier material decreases compared to the distance in the paint changing the proportion a_n subsection 3.3.2 and therefore the combined attenuation length. So the attenuation in the paint gets more relevant for smaller geometries.
In the following, we investigate how the overall attenuation is affected assuming different thicknesses and attenuation lengths for paint layer and carrier material.

5.2 Attenuation in the oWl Fiber

5.2.1 Propagation

To understand how much the light in the oWl-fiber is attenuated in each of the two layers, we need to understand how the captured light moves through the fiber.

Flattened Model

First we consider the simpler case where we only have one material with one attenuation length λ_{Bulk}. In general, the number of photons $N(d)$ as a function of the distance travelled $d_{travelled}$ follows a Lambert-Beer-Law as presented in Eq. 5.1.

$$N(d) = N_0 exp\left(-\frac{d_{travelled}}{\lambda_{Bulk}}\right). \tag{5.1}$$

To calculate the travelled distance of the captured photons, we look at the generated photons in spherical coordinates (analoguos definitions as in section 4.1), aligning the symmetry axis of the optical fiber with the z direction (see Fig. 5.2). Here, the angle θ describes the movement along z and the φ angle describes the angle with the surface normal of the cylinder wall.

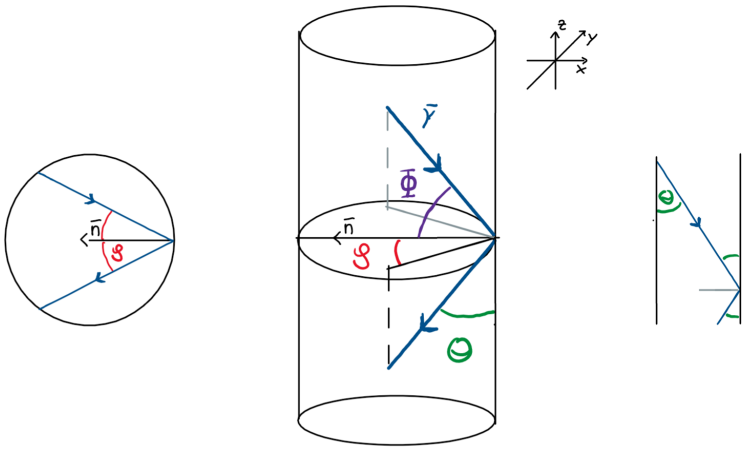

Fig. 5.2.: Choice of polar coordinates to describe photon propagation in the oWl-fiber. The origin is located at the edge of the cylinder. The polar angle θ describes the deviation from the fiber direction and thus describes the movement along the fiber direction (right). The azimuth angle φ describes the deviation from the surface normal and thus the movement in the fiber cross-section (left)

So the distance a photon needs to travel from its starting point to one of the two ends depends on its movement along the fiber direction (here further in the z direction), and thus on its polar angle θ. The effective distance that is travelled to overcome the distance z along the fiber is given by:

$$d_{eff}(\theta) = \frac{z}{cos(\theta)} \tag{5.2}$$

combined with the bulk attenuation Eq. 5.1 we obtain for the one sided efficiency:

$$\varepsilon_{one}(z) = \frac{1}{2\pi} \int_{-\frac{\pi}{2}}^{0} d\theta \int_{-\frac{\pi}{2}}^{\frac{\pi}{2}} d\varphi \; H(\theta,\varphi) \; sin(\theta) \; exp\left(-\frac{z}{cos(\theta) \; \lambda_{Bulk}}\right) \tag{5.3}$$

With $H(\theta,\varphi)$ being the Heaviside function that describes the angles under which a photon is captured.

$$H(\theta,\varphi) = \begin{cases} 1: & captured \\ 0: & not\ captured \end{cases} \tag{5.4}$$

This approach to describe the measured intensity was introduced as the so called flattened model[1] in the course of the WOM development to analytically describe the attenuation in the WOM-Tube. This model works relatively well, as long as the assumption of a single bulk absorption length for both paint layer and tube holds.

Paint Model

To get a more precise model the paint layer has to be taken into account. In order to obtain the influence of the attenuation in the paint on the overall attenuation, the relative distance in the paint must be determined. For this purpose we only have to examine the propagation in the cross section plane Fig. 5.3. And due to the symmetry of the rod, the photons retain their angle φ to the normal vector and fiber direction θ. This means that only the path between two reflections needs to be considered, which can be transferred to all subsequent reflections.

The azimuth φ, sketched out in Fig. 5.3, describes the movement in the cylinder cross section plane and therefore the proportion of the distance travelled in the paint $p_{Paint} = \frac{s_{paint}}{s_{total}}$. To calculate the distances, we consider the substrate as an inner cylinder with a radius of b surrounded by another outer cylinder with a radius of r_0 which represents the outer radius of paint layer. Now we consider a photon at the edge of the outer cylinder which moves through the plane at the angle φ and calculate the distance s to the intersection points with the cylinder walls.

[1] more elegantly introduced in [3]

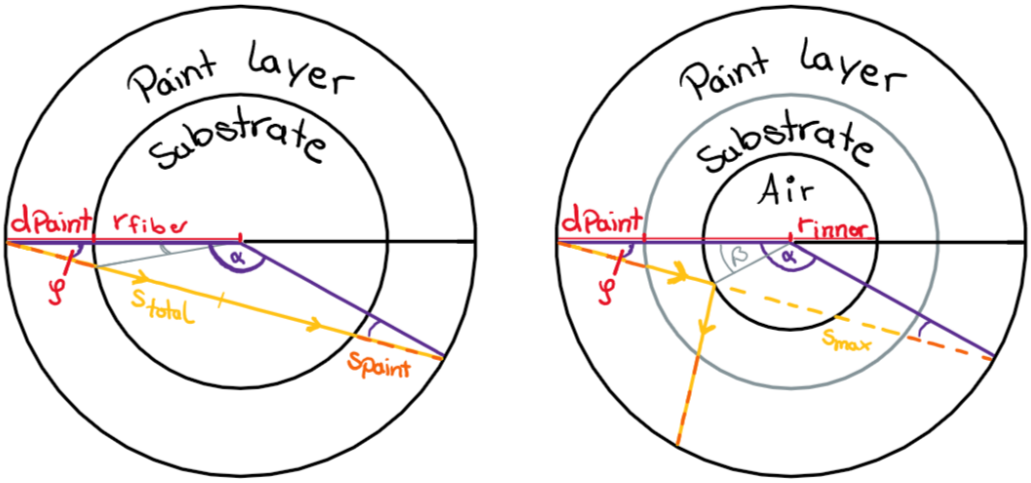

Fig. 5.3.: The path length that a photon travels in the plane from one reflection to reflection s_{total} and in the WLS-paint s_{paint}, dependent on φ. On the left the case of a solid cylinder with radius r_{fiber} and a d_{paint} thick WLS-paint layer at the outer surface. The intersection point of the light path and the substrate is described by the substrate radius and the angle β. On the right hand the case of a hollow cylinder is shown. The photons that hit the inner substrate wall r_{inner} are reflected back to the paint reducing the distance between reflections on the outer surface leading to an increase of the distance fraction spend in the paint layer.

$$\begin{aligned} \vec{s} + \vec{r_0} - \vec{b} &= 0 \\ (\vec{s} + \vec{r_0})^2 &= \vec{b}^2 \\ \vec{s}^2 - |\vec{r_0}|\,|\vec{s}\,|cos(\varphi) + \vec{r_0}^2 &= \vec{b}^2 \end{aligned}$$

$$s_{\pm} = r_0 \left(cos(\varphi) \pm \sqrt{cos^2(\varphi) - 1 + \frac{b^2}{r_0^2}} \right) \tag{5.5}$$

To calculate the total distance in an outer circle, we only have to calculate the distance to the first intersection s_- and use the symmetry of the circle. Therefore s_{outer} is equal to $2\,s_-$

If the path does not cross the inner circle and therefor does not leave the outer circle, the distance travelled in the outer layer is the distance to the next wall s_{max}

$$s_{outer} = \begin{cases} 2\,s_- & : \; 0 \leq cos^2(\varphi) - 1 + \frac{b^2}{r_0^2} \\ s_{max} = 2\,r_0\,cos(\varphi) & : \; 0 > cos^2(\varphi) - 1 + \frac{b^2}{r_0^2} \end{cases} \tag{5.6}$$

This can be used to calculate the distance in the paint s_{Paint} with $b = r_{fiber}$. In case of a hollow cylinder where the light will be reflected at the inner cylinder wall, the total travelled distance will be reduced as shown in Fig. 5.3. The total distance in the cross section plane can be calculated in the same way we calculated s_{Paint}: s_{total} with $b = r_{inner}$. The resulting distributions for the WOM-Tube geometry and an oWl-fiber are shown in Fig. 5.4.

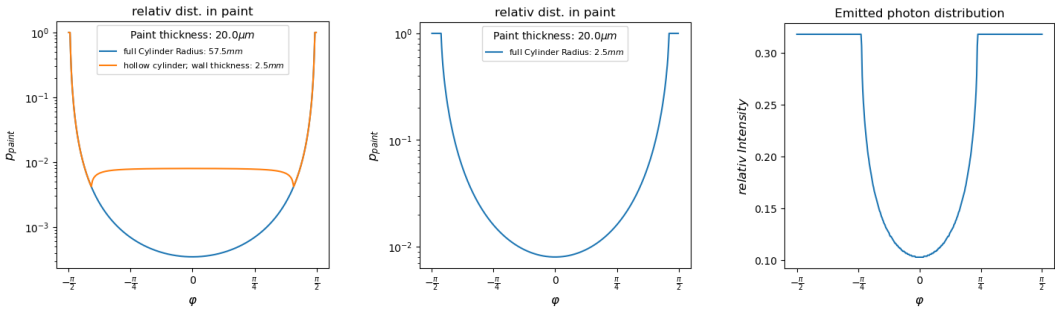

Fig. 5.4.: The left and middle plot shows the relative distance in the paint layer dependent of φ for different geometries. In the left for the geometry of the WOM-Tube (orange) and a full cylinder with the same radius (blue) is shown. The middle plot shows the distribution for a 5 mm rod. As expected rises the portion in the paint for the smaller geometries giving the paint more influence. If one now looks at the right plot of the distribution of captured photons for an PMMA based oWl fiber in φ most of the photons are emitted at an angle over $\frac{\pi}{4}$ to the normal vector amplifying the effect.

Now we can use Eq. 5.7 to calculate the effective attenuation length λ_{eff} for a photon for different attenuation lengths in the paint and carrier material (see Eq. 5.7).

$$\lambda_{eff}(\varphi) = \frac{\lambda_{Paint}\ \lambda_{Bulk}}{\lambda_{Paint}\ p_{Bulk}(\varphi) + \lambda_{Bulk}\ (1 - p_{Bulk}(\varphi))} \tag{5.7}$$

Integrating the effective attenuation length Eq. 5.7 into the flattened model Eq. 5.3 gives us the so called paint model Eq. 5.8. For simplicity, we assume that the refractive indices (1.46 for quartz glass and 1.49 for the paint) of the layers are identical. This neglects the possibility of total internal reflection at the layer boundary. This effect should however only affect few photons and therefore have a minor impact on the overall distribution.

$$\varepsilon_{one}(z) = \frac{1}{2\pi} \int_{-\frac{\pi}{2}}^{0} d\theta \int_{-\frac{\pi}{2}}^{-\frac{\pi}{2}} d\varphi\ H(\theta, \varphi)\ sin(\theta)\ exp\left(-\frac{z}{cos(\theta)\ \lambda_{eff}(\varphi)}\right) \tag{5.8}$$

So the possibility of scaling down the geometry depends on the difference in the attenuation lengths of the layers.
An one indication for this effect is the relative "bad" attenuation length for the WOM-Tube of $3\,\mathrm{m}$ to $5\,\mathrm{m}$. Since the WOM-Tube is made of high purity quartz glass [2] the attenuation length is assumed to be at least $20\,\mathrm{m}$ Fig. A.1. In order for the combined attenuation length to be reduced from 20 to 5 m, the attenuation length in the paint must be in the order of cm. Using the same values of attenuation for a $5\,\mathrm{mm}$ diameter fiber, the effective attenuation length is further reduced as is shown in Fig. 5.5. This would lead to large attenuation losses in small fibers.

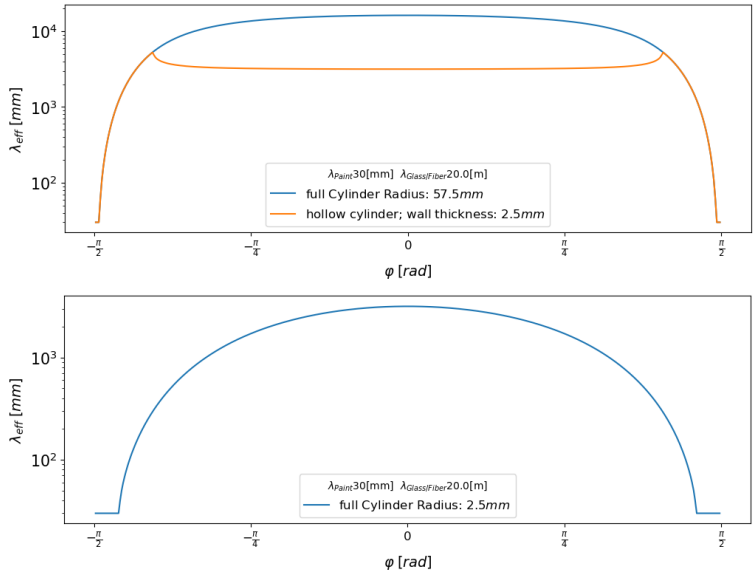

Fig. 5.5.: Change of the attenuation length for different geometries at the top: The geometry of the WOM-Tube and a full cylinder variant and on the bottom. The attenuation length of a 5 mm fiber with the same paint layer.

Conclusion

The following information was obtained for the different parameters: For a relative decrease of the substrate thickness to the paint thickness the capture rate decreases. However, this effect only becomes relevant when the substrate fall in the same order of magnitude as the paint thickness.
In the case of the attenuation length, shrinking makes a difference if the attenuation lengths of the paint and substrate materials differ significantly. This effect varies for different emission angles and could lead to a change of the signal shape and

[2] HSQ® 300 from Heraeus [@12]

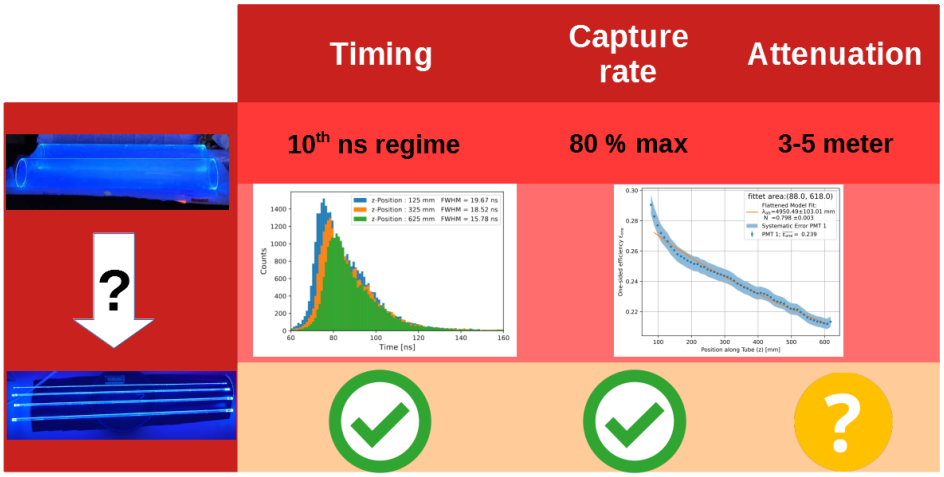

Fig. 5.6.: Transferability of the WOM-Tube to smaller geometry

therefore the timing. However, the effect on the timing was neglected here, as it is considered small compared to the overall signal. And the focus is on the attenuation, as an increase here can negate the gain from the capture rate.

5.3 Attenuation Measurement

In order to check for the effect in the paint we can measure the attenuation for different geometries.
To measure the attenuation, we utilize the property of the wavelength-shifting fiber to capture and couple light. Therefore, we can measure the intensity at different distances. For this purpose, the setup for testing the WOMs was used Fig. 5.7, which measures the intensity as a function of the distance to the illumination point.

5.3.1 Setup

As light source a Xenon lamp for light in the broad UV spectrum and a monochromator are used. Thus we can choose light for illumination from a spectrum from $250\,\mathrm{nm}$ up into to the infrared regime. Fluctuations in the intensity of the lamp are corrected by splitting the light with a beam splitter in two beams, sending one onto a reference photo diode. The remaining light beam is guided into a dark box via liquid light guide (LLG). In the dark box, the fiber/tube is mounted along a rail. The end of the LLG can be moved along the rail to vary the illumination point and distance

to one end, where a readout PMT records the signal amplitude. It is also possible to rotate the light guide around the fiber. The remaining light at the end of the fiber is detected with a PMT coupled with a silicon based optical gel. To reduce errors from back reflections at the non-measured side, the other end can be coupled to either a second PMT or a black end cap. The signals from the measuring PMT and the reference diode are read out with two lock-in amplifiers that use a chopper signal as a trigger. The chopper is located in front of the beam splitter. In this way, the signal is measured for the case of an interrupted and not interrupted beam, allowing automatic background subtraction.

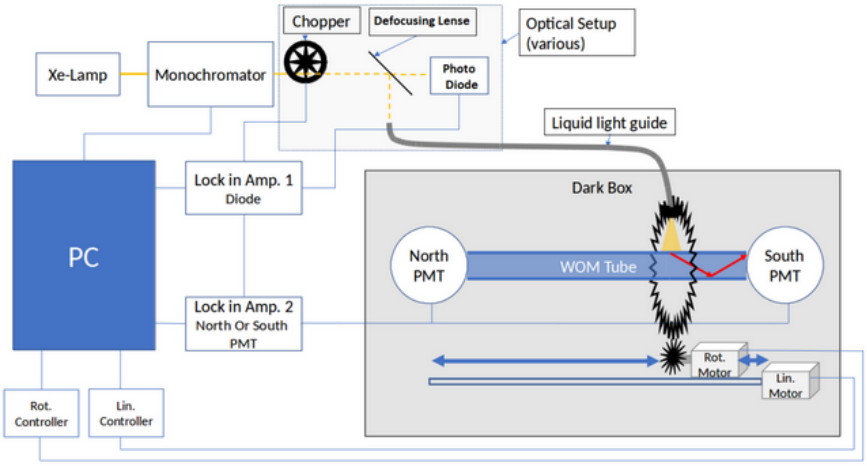

Fig. 5.7.: Design of the WOM test stand. Taken from[13]

5.3.2 Measurement

A computer is used to take the measurement, which controls the monochromator, the motors and reads the data from the lock-in amplifiers. The data is then corrected for fluctuations in the lamp and the background. To determine the attenuation, this is sufficient.
To determine the absolute efficiency, the data must still be corrected for the quantum efficiency (QE) of the PMT and the absolute intensity with which the fiber is illuminated. The absolute intensity is obtained by illuminating the PMT directly with the LLG and correcting for the QE of the PMT. A more detailed description of the corrections especially for the efficiency measurement of the WOM-Tube can be found in [14][3].

[3] may not yet be published, alternatively one can look into [13] to get a feeling (partially outdated).

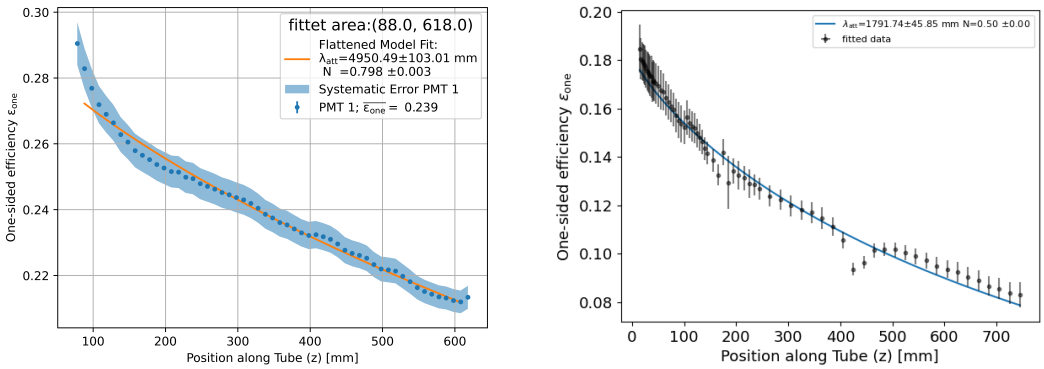

Fig. 5.8.: Intensity curve for the WOM-Tube and a 6mm oWl fiber, both coated with an approximately $16\,\mu\mathrm{m}$ thick paint layer. The flattened model was fitted to the data 5.3. If the paint layer would not play a major role, both measurements should result in comparable attenuation lengths. For the oWl fiber, however, the attenuation length is significantly shorter.

5.3.3 WOM to oWl-Fiber

This setup can now be used to compare the intensity curve of the WOM-Tube with that of a oWl-fiber. For this purpose, a $6\,\mathrm{mm}$ diameter quartz rod was coated with wavelength-shifting paint and measured in the test stand. The effective bulk attenuation was determined by fitting the flattened model to the data and the attenuation lengths were compared. The tube developed for the WOM achieves an effective absorption length of around $5\,\mathrm{m}$, compared to commercial fibers with around $3\,\mathrm{m}$ [@9], this is a good value. The value determined for the oWl-fiber, on the other hand, is only $1.8\,\mathrm{m}$ Fig. 5.8. This indicates the effect described in subsection 5.2.1 of a high attenuation in the paint and the resulting higher attenuation for smaller geometries.

The assumption that the paint significantly attenuates the light seems to be correct. The question now arises about the cause of the high attenuation and whether this can be influenced to save the idea of the oWl-fibers.

6 The outer Layer

In this chapter, we investigate the reason for the high attenuation in the paint. We will discuss the composition, the method of applying the paint, as well as the possibility of clumping and self-absorption of the wavelength-shifting molecules in the paint.

6.1 WOM Paint

The so-called WOM paint Fig. 6.1a used to create the paint layer, forms the actual detector area where the high-energy photons are absorbed, shifted, reemitted and trapped. For this purpose, the thickness and wavelength shifter concentration must be chosen to absorb the majority of the desired incoming spectrum. In order to keep the reemitted photons, the overlap between absorption and emission spectrum should be as small as possible and also have a homogeneous surface, to avoid disrupting the photon guidance along the fiber.

The WOM-paint base is a transparent plastic (PEMA) acting as the carrier matrix for the wavelength shifters, both dissolved in the solvent toluene. After application on the substrate (fiber or tube), the paint solidifies as the solvent evaporates.

6.1.1 Composition of the Paint

Solvent

To mix the solid matrix with the wavelength shifters and to apply them on the tube we use a solvent to liquefy them. The main requirement for a solvent is its capability to solve both in the desired concentration. Also, the solvent should have a low evaporation rate at room temperature such that the concentrations don't change during storage. Also a too volatile solvent results in air bubbles during drying process.

Fig. 6.1.

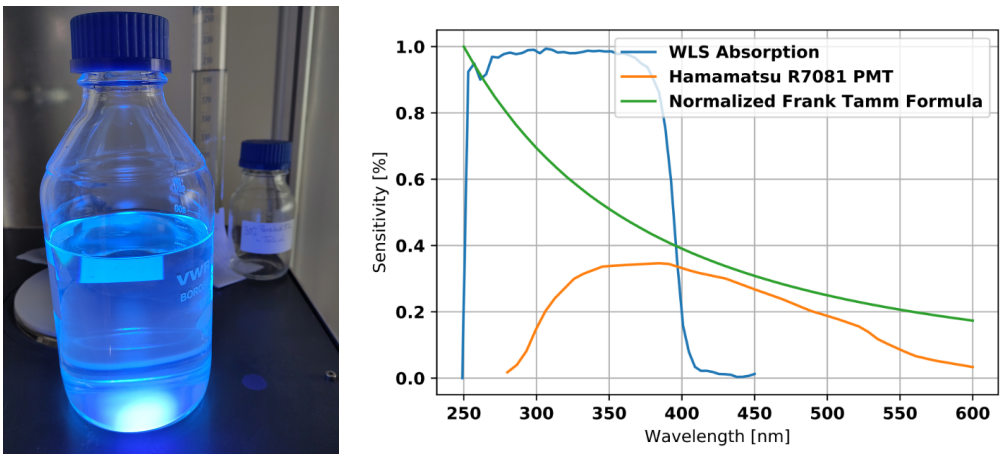

(a) WLS paint, illuminated with a UV lamp.

(b) Absorption spectrum of the WOM paint compared with the QE of the PMT (Data sheet: [@15]) used in the DOMs and the Cherenkov spectrum (normalized Frank Tamm formula [13]). The WOM-paint can absorb a larger part of the Cherenkov spectrum due to its sensitivity for smaller wavelength compared to the PMT of the mostly used modules in IceCube. Taken from [13].

For the WOM-paint toluene is used, acetone also was considered but rejected due to the high volatility.

Matrix

As matrix for the wavelength shifters, we need a transparent material with a similar refractive index as the carrier material to avoid interface effects.
For the WOM-paint, Poly(ethyl methacrylate) (PEMA) [3] is used. Also, other transparent plastics like PMMA or Polystyrene would be possible.
The concentration of PEMA in the solvents defines the viscosity η of the paint. For higher concentrations the paint gets more viscous. For the WOM-Paint the ratio of $22\%_{mass}$ to $78\%_{mass}$ toluene was set experimentally [16].

Wavelength Shifter

The used wavelength shifter defines the absorption spectrum of the fiber. The absorbance A of the paint layer can be changed by adjusting either the paint thickness d or the concentration of the wavelength shifter c using the mass extinction ε_{mass}, from Beer´s Law presented in Eq. 6.1.

$$A = -log_{10}\left(\frac{I}{I_0}\right) = \frac{d \cdot c \cdot \varepsilon_{mass}}{log(10)} \tag{6.1}$$

For a combination of two or more wavelength shifters, we get an increase in the overall absorbed spectrum. However, two aspects must be taken into account. First, even when using a shifter with a high quantum yield (QY), every time the photon is shifted this QY has to be accounted leading to higher losses for the lower shifters.

Secondly, the light that gets absorbed by the lower shifter will be reemitted isotropically. Therefore a fraction of re-emitted photons will no longer fall under the TIR condition. If the captured light gets now absorbed from the upper shifter the same fraction will be lost again due to the TIR condition. So photons that are shifted multiple times will be reduced additionally. This effect can be reduced if the concentration of the upper shifter is high enough that the emitted light of the lower shifter gets absorbed before it can leave the fiber. Therefore only for the last shifter the capture rate comes into account.

For testing the fibers we used the WOM-Paint, which is designed for a broad absorption in the UV-region ($250\,\mathrm{nm}$ to $400\,\mathrm{nm}$). For this purpose the paint contains 1.3 g/l of Bis MSB and 2.6 g/l P-terphenyl. So the WOM gets the desired broad absorption spectrum shown in Fig. 6.1b and the effects of multiple shifters are reduced. Also considering Eq. 6.1 the paint layer can be small which is important for the capture rate Fig. 4.5.

Name	Toluene	PEMA	Bis-MSB	P-terpheny
WOM-paint (OldP64)	$78\%_{mass}$	$22\%_{mass}$	1.3 g/l	2.6 g/l

Tab. 6.1.: Composition of the WOM-paint.

6.2 Application of the Paint with Dip-Coating

In order to achieve consistent paint thicknesses and even surfaces, the dip coating process is used for the production of the WOMs and also the test-oWl-fibers. In this process, the carrier is submerged vertically in the paint and removed at different velocities depending on the desired paint thickness and the viscosity Eq. 6.2.

$$d_0 = 0.8 \cdot \sqrt{\frac{v_{coating}\,\eta}{\rho}} \tag{6.2}$$

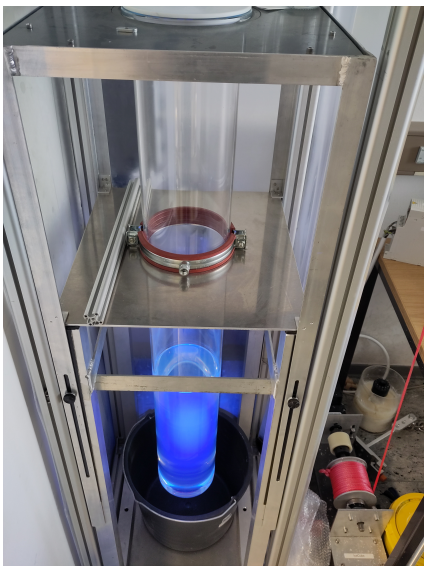

Fig. 6.2.: Picture of the Dip-coater and the paint bath illuminated with UV ligth

For the coating itself, a customized stand is set up for the production of the WOM-Tubes, which is also used for coating the smaller oWl-fibers Fig. 6.2. The stand has a $1\,\mathrm{m}$ deep paint reservoir. The test samples can be submerged into the paint and removed using a flask puller with motor. For the used paint Table 6.1, thicknesses from $10\,\mu\mathrm{m}$ to $80\,\mu\mathrm{m}$ are possible. Measurements of the surface quality of coated slides showed that the fluctuations in the surface are less than $100\,\mathrm{nm}$ and thus small enough that the surface is flat for the trapped photons with a wavelength above $100\,\mathrm{nm}$. Fig. 6.3. So a problem with the surface and the resulting increase in attenuation seems not to be an increasing factor for the attenuation.

For detailed information about the theory of Dip-coating and the calculation of the paint layer thickness, it is recommended to read the following thesis [17].

6.3 Clumping of Wavelength Shifters in the Paint

Since the shifting properties of a wavelength shifter depend on the energy levels of the molecular bonds, which can be influenced by intermolecular forces. For example, the position of the absorption peak can be shifted by the choice of solvent Fig. A.2. But wavelength shifters also influence each other depending on their spacing and thus their concentration. Such that at high concentrations the shifters start clumping [18].

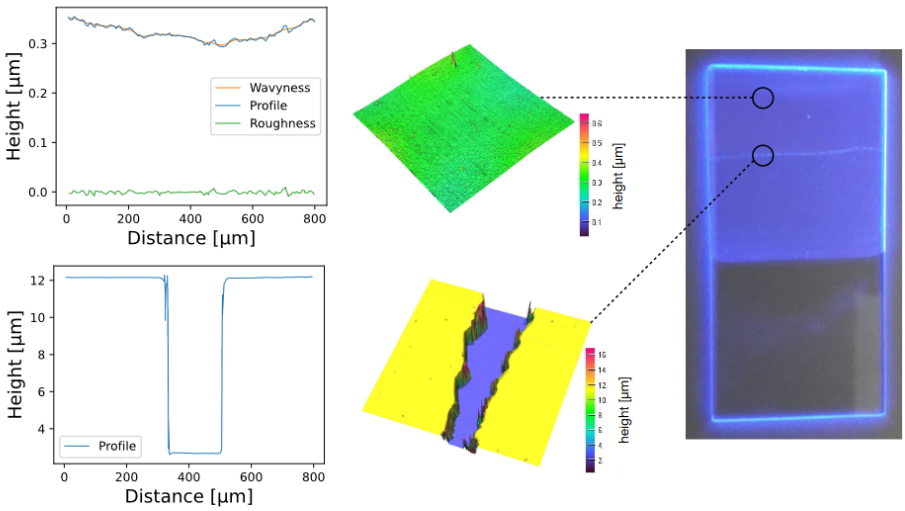

Fig. 6.3.: Profilometer measurements of two different paths on a slide, coated with the wavelength shifter, are shown. In each row the measured profile is shown on the left and a 3 dimensional profile is shown in the middle. The path in the bottom row comprises a scratch in order to measure the thickness of the coating. A photograph of this slide is shown on the far right in which the approximate measurement points are indicated. Image and text from [3]

6.3.1 Clumping

Clumping occurs when the solvent is not "strong" enough to separate the wavelength-shifting molecules, allowing them to stack in chains. This stacking prevents the molecules inside the chain from working as wavelength shifters, as they are in the shadow of others in the chain, such that only the outermost molecules contribute as a wavelength shifter. For higher concentrations, these chains will increase further, breaking the linearity of absorbance and concentration described in Eq. 6.1, since the new molecules mainly enlarge the chains where only a few new shifting centers are created Fig. 6.4. Furthermore, these structures can become scattering centers when they reach the size of the lights wavelength Fig. 6.5 and additionally increase the attenuation in the paint. Eq. 3.3

6.3.2 Testing for Clumping

In order to check if clumping disturbs the light transmission in the paint we test for the linearity from Eq. 6.1 by calculating the linearity constant for different concentrations. For this purpose, samples with different concentrations are tested for their absorbance. The concentration ranged from a few mg / l of Bis-MSB up to the used concentration in the paint of 1.3 g / l. To measure the absorbance, a

Fig. 6.4.: Effect of clumping on the absorption properties of the wavelength shifter

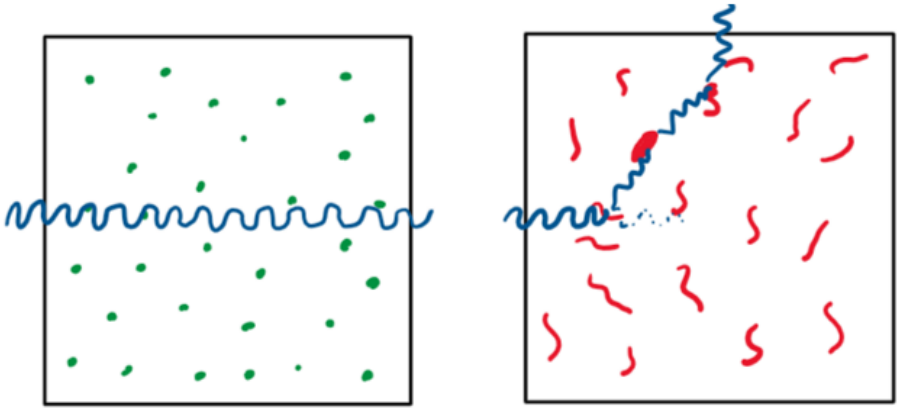

Fig. 6.5.: Effect of clumping of the wavelength shifters. On the left, no clumping occurs and the medium is transparent. On the right, the shifters form larger structures where the light can scatter.

UV-Vis spectrometer[1] is used, which measures the absorbance of a sample in the wavelength range from $250\,\mathrm{nm}$ to $800\,\mathrm{nm}$. With the absorption we can calculate the mass extinction coefficient ε_{mass} with Eq. 6.3.

$$\varepsilon_m = \frac{A \cdot ln(10)}{d \cdot c} \tag{6.3}$$

Setup

The used UV-Vis can measure samples in a $10\,\mathrm{cm}$ or $1\,\mathrm{cm}$ cuvette. It is equipped with a tungsten-halogen and deuterium lamp, a monochromator and a PMT which detects the transmitted light Fig. 6.6. Allowing the device to measure an absorbance of up to 8, which corresponds to a transmission of 1e-8 [@19].

[1] Lamda 850 from Perkin Elmer[@19]

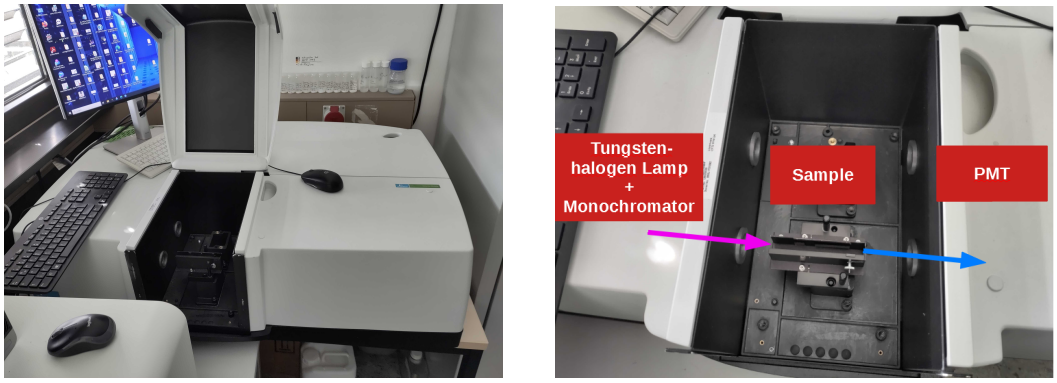

Fig. 6.6.: The UV-Vis [@19] used, with the light path shown.

However, measurements with relatively highly concentrated wavelength shifters, starting from 3 mg / l Bis-MSB, show that the device saturates Fig. 6.7 at an absorbance of 3. This can be explained by the fact that the measured wavelength shifters re-emit the absorbed light. Since the PMT cannot distinguish between transmitted and emitted light, the emitted light is measured as transmitted light. Limiting the device to an maximum of 3 for the absorbance.

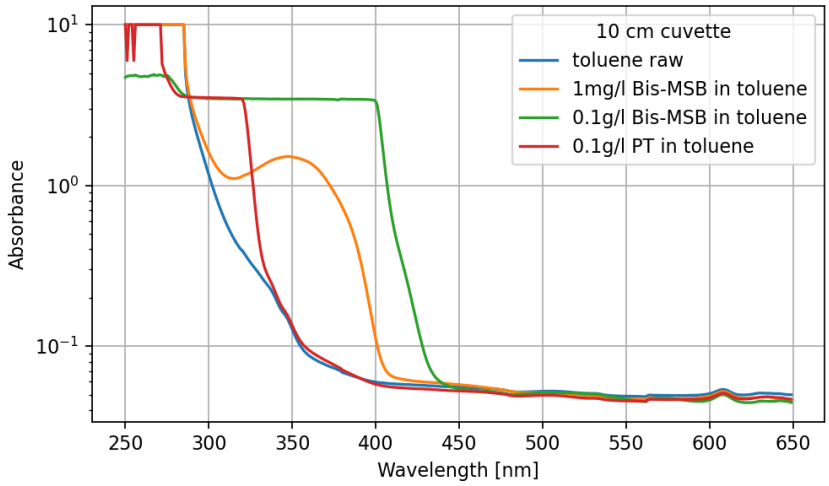

Fig. 6.7.: Absorbance spectra of the wavelength shifters used in the WOM-paint dissolved in toluene. In the absorption spectra of p-Terphenyl(PT) and Bis-MSB for the 100 mg / l measurement the UV-Vis saturates already at 3 due to the reemitted photons.

The range of interest lies for the concentration in the gram per liter range, far above the saturation limit we saw in Fig. 6.7. In order to remain below the limit, the absorbance must be reduced for the same concentrations so the samples must become thinner. From Fig. 6.7 it can be estimated that a cuvette must be at least

200μm thin such that the absorbance maximum at a concentration of one gram per liter is below 3 and can therefore be resolved by the UV-Vis.

For this purpose, custom cuvettes made by gluing two soda-lime glass carriers together with a wire as spacer Fig. 6.8. The width of the cuvettes are measured using a micrometer screw achieving a thickness of $300\,\mu\mathrm{m}$. This is not sufficient to measure the desired maximum concentration. For this reason, two fully glued "cuvettes" were also produced. These use a plastic ring as a separator in which the sample is fully confined. The thickness achieved for these two is around $150\,\mu\mathrm{m}$.

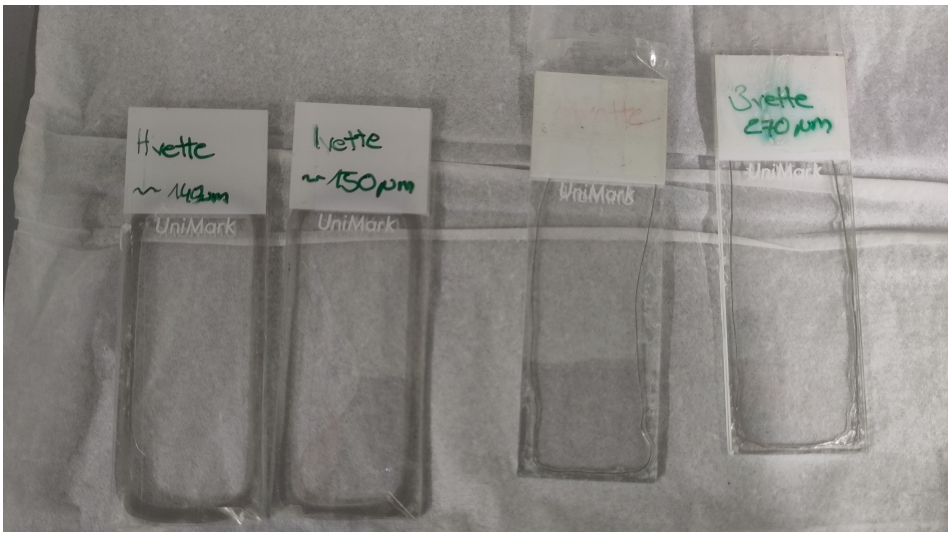

Fig. 6.8.: Custom made cuvettes made out of two soda-lime glass carriers and a spacer. The two on the left are fully sealed and the two on the right are open at the top for refill.

Measurement

For the broader cuvettes in the $300\,\mu\mathrm{m}$ range, solutions with concentrations in the range of $100\,\mathrm{mg}$ to $800\,\mathrm{mg}$ Bis-MSB per liter solvent are prepared. As solvents Acetone and toluene are used. Cyclohexane also was considered and prepared, but it turned out that cyclohexane cannot dissolve a concentration of 1000 mg / l. Additionally, a reference solution of 100 mg / l in dichloromethane is used, as it is strong polar due to the two chlorine atoms and therefore no clumping is expected here, making it a suitable reference.
Four measurements series are taken using one cuvette for each series, two with toluene and two with acetone.
First we start with the measurement of the baseline absorbance, containing the

absorbance from the cuvette and the solvent for each series. Although the cuvettes were cleaned with their respective solvents after each concentration run, complete removal of residues is not possible due to the small spacing of the cuvettes [2]. So in order to reduce the effects of possible contamination the different concentrated solutions are measured from low to high concentration.

To measure the high concentration range, a reduced version of the WOM-paint without the lower shifter P-terphenyl was used, which therefore only contains 1.3 g / l Bis-MSB. Since this probe has a higher viscosity due to the contained PEMA it could be sandwiched between the soda-lime glass carriers.
For each concentration the cuvettes are placed in a custom made holder and measured 5 times per concentration. Fig. 6.9

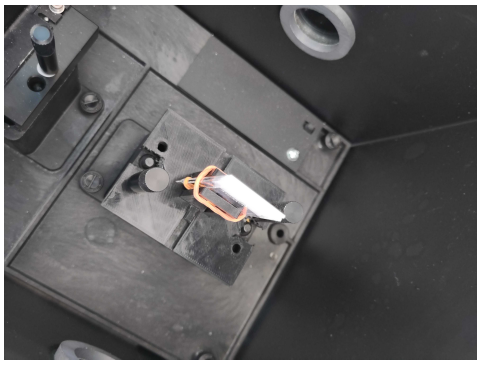

Fig. 6.9.: Image of a custom-made cuvette placed in the UV-Vis.

Results

The measured data are corrected for the baseline, whereby the toluene baseline from the "G" measurement was used for the fully sealed cuvettes. With the corrected absorbance, the cuvette width and the concentration, we calculate the mass extinction ε_{mass}, which can be compared for the different concentrations Fig. 6.10. Looking at the measurements, we see a difference between the solvents for the shape and the position. Which can be explained by intermolecular forces between the shifters and the solvent. For the different concentrations, the spectra lie well above each other up to the 400 mg / l measurement. However, the peaks for the 600 mg / l and 800 mg / l samples are apparently already at the saturation limit and therefore can no longer be fully resolved. Nevertheless, the shape of the peaks at their rising slope can be compared with the smaller concentrations. The peak for the 100 mg / l

[2] This can be clearly seen in the subsequent measurement of the baseline Fig. A.7

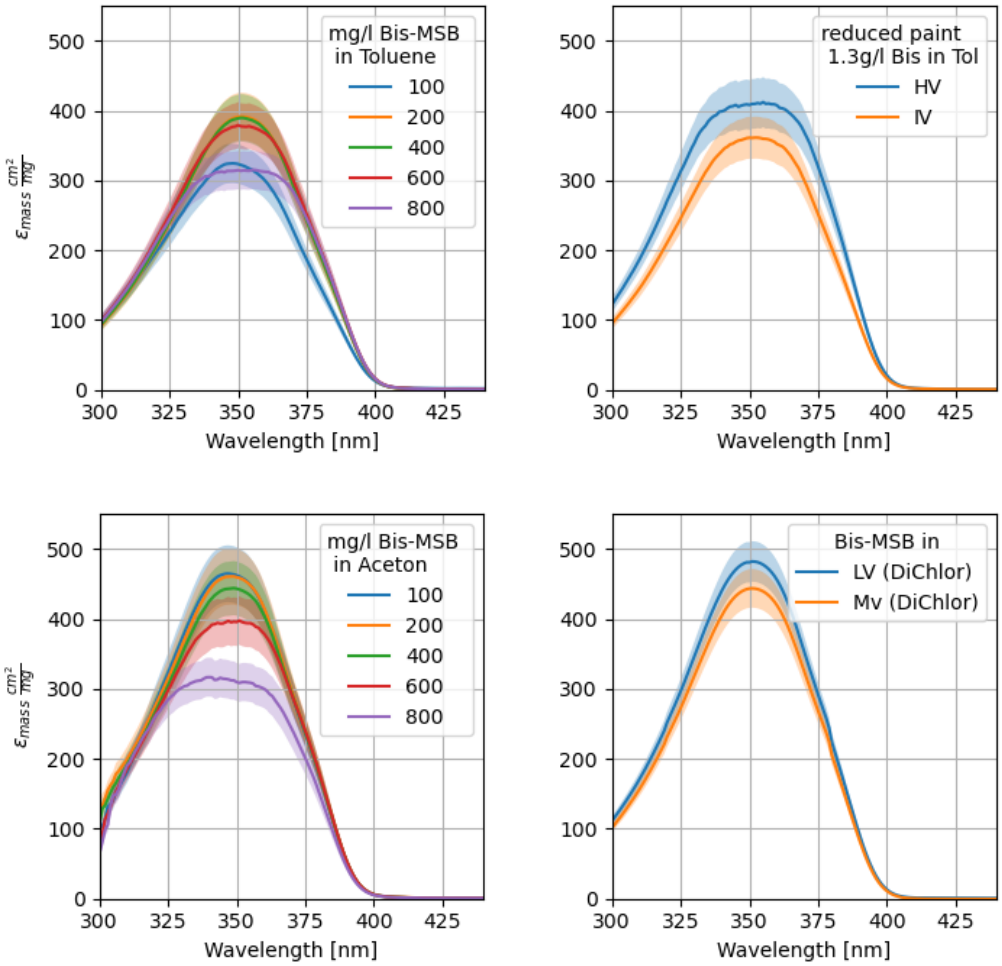

Fig. 6.10.: Results of the clumping test. The full measurement results can be found in Appendix A.

in toluene measurement is slightly below the measurement results, this could be explained by an error in the process of diluting the samples, as this effect occurs in both toluene samples Fig. A.5 and Fig. A.6.

Looking at the extinction coefficient. Acetone is with $450\,\mathrm{cm}^2\,\mathrm{mg}^{-1}$ $\frac{cm^2}{mg}$ slightly higher than toluene with $400\,\mathrm{cm}^2\,\mathrm{mg}^{-1}$. However, both are in agreement with the reference measurement of dichloromethane. Looking at the extinction coefficient for the 1300 mg / l paint, it is also in the range of the probes with a low concentration. So a change of the extinction coefficient could not be shown in the measured concentration range. Therefor we don´t have any indication of a reduction in the absorption due to clumping.

6.3.3 Light Yield

It was shown that the absorbance increases with the concentration as expected. In addition, it is also to be shown that the amount of emitted photons increases with absorption. To test this, the light yield shall also be measured over several concentrations.
Here, a fluorospectrometer[3] Fig. 6.11a is used, which can illuminate a sample at certain wavelengths using a xenon lamp and a monochromator. The emitted light spectrum is measured using a second monochromator and a PMT Fig. 6.11b

Fig. 6.11.

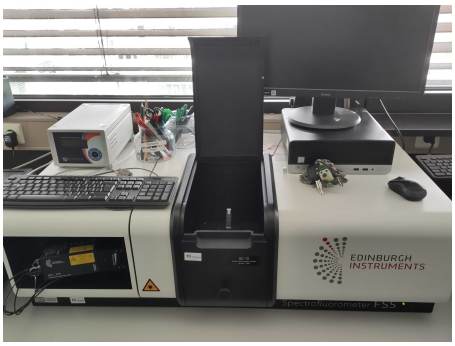

(a) FS5

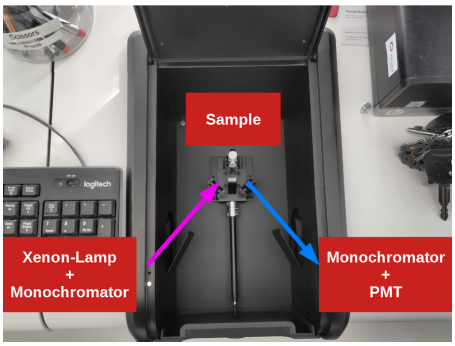

(b) FS5 - front face holder

Theory

A major problem with such measurements is the self-absorbance of wavelength-shifting materials, which always have a certain overlap of the emission and absorption spectrum section 2.2. A higher concentration leads into a greater absorption of the emitted light and can corrupt the measurement. To prevent the spectrum from being influenced by the concentration, the sample is observed from the same side as it is illuminated. Fig. 6.12. In this way the distance that the photon has to travel to leave the sample is the same it took it to be absorbed. We can determine the absorbance of an emitted photon as a function of the absorbance of the exciting photon Eq. 6.5. Here we see that the absorbance is no longer dependent on the concentration used. Thus, the spectra can be compared with each other.
This is also shown in a simulation of an illuminated sample and the resulting emission spectrum, where the shape was compared for different concentrations. Fig. 6.13.

[3](FS5[@20])

$$A_{emm}(\lambda) = log(10)\ d\ c\ \varepsilon(\lambda)\ ;\ d = \frac{A_{absorbt}}{c\ \varepsilon(\lambda_{exite})\ log(10)} \tag{6.4}$$

$$A_{emm}(\lambda_{emm}) = A_{absorbt} \frac{\varepsilon(\lambda_{emm})}{\varepsilon(\lambda_{exite})} \tag{6.5}$$

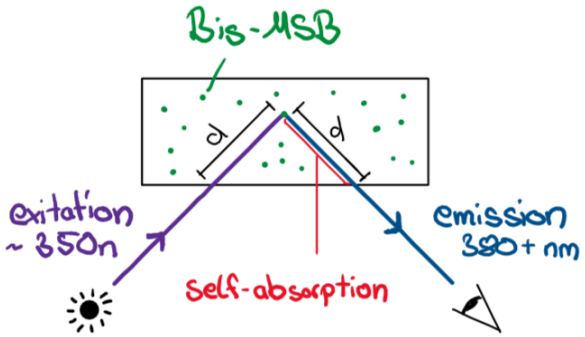

Fig. 6.12.: Light path for the front face setup.

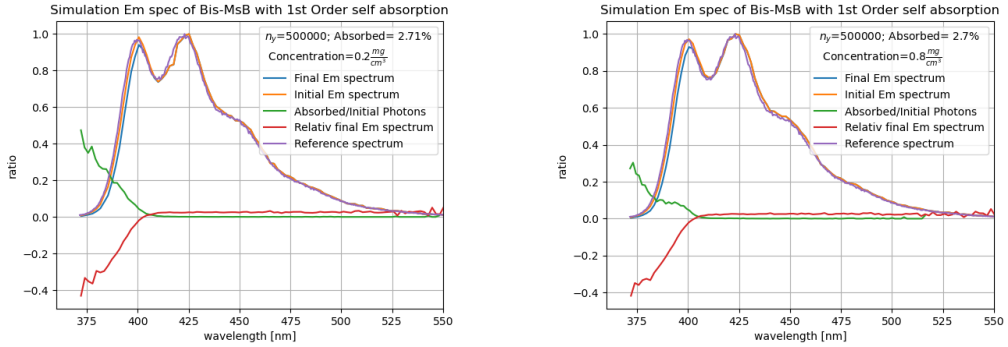

Fig. 6.13.: Simulation of a sample illuminated and measured from the front for different concentrations. The emitted spectrum is reduced by the self-absorption of the shifter for lower wavelengths. However, the total amount of absorbed photons and the final spectrum is independent of the concentration. A measurement of the reference spectrum and a high concentrated probe is shown here Fig. A.16

Results

The amount of detected light is constant over all samples and concentrations Fig. 6.14.

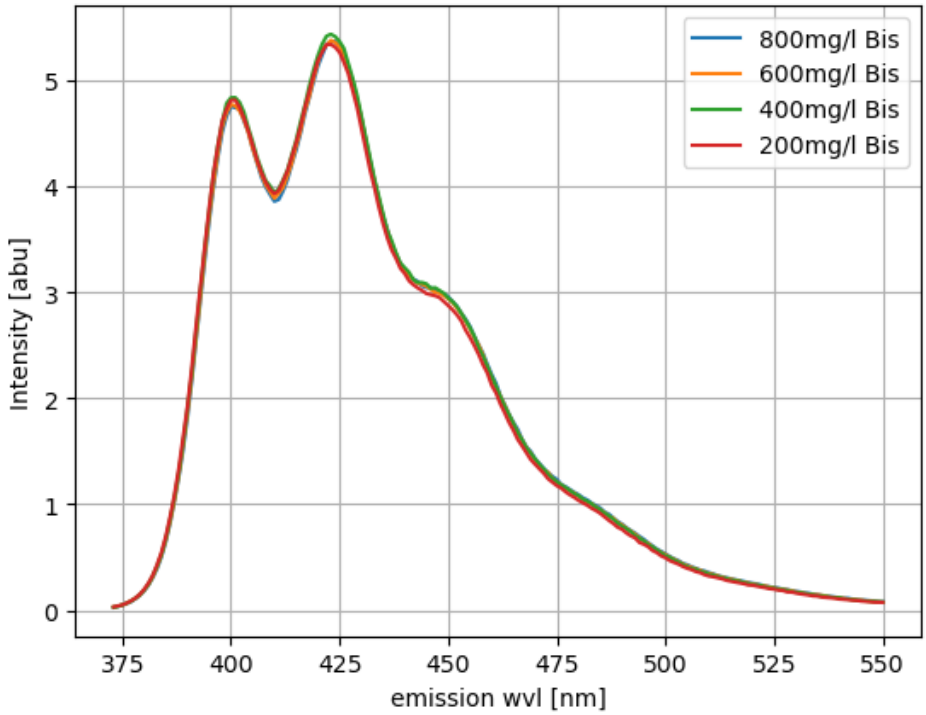

Fig. 6.14.: Emission spectrum for different concentrations of Bis-MSB. Measured with the FS5 front face sample holder

6.3.4 Results for Clumping

Taking the results of subsection 6.3.2 and of subsection 6.3.3 together, the absorbance increases linearly according to Beer´s Law Eq. 6.1 without losing light. Clumping effects can therefore be excluded for the tested solvents and concentrations. Therefore, they are also not an explanation for the high attenuation in the paint and don´t leave a room for improvement. On the positive side, the concentration of the wavelength shifters can be varied within a wide range without any fear of a loss in performance.

6.4 Self-Absorbance

In the course of the investigation for clumping effects, the influence of self-absorption on the light yield measurement was analyzed. It was found that this effect can be neglected for the measurement, but if you look at the expected final spectrum and compare it with the initial spectrum, there is a difference of $\tilde{3}5\%$ for photons with a wavelength below $400\,\mathrm{nm}$ Fig. 6.13. Thus, the wavelength shifter could be a driving factor for the high attenuation in the fiber due to its self-absorption.

6.4.1 Self-Absorbance

As explained in section 2.2 self-absorption is the result of the overlap of emission and absorption spectrum, allowing the wavelength shifter to absorb a part of its emitted light. The self-absorption behaves in general as the regular absorption. However, for the fiber, this effect also means that the photon that get absorbed via self-absorption can be reemitted. They receive a new wavelength and a new direction of movement. If this falls below the TIR condition again, they remain trapped and are therefore not automatically lost. The probability that the photon is "preserved" is given by the QY of the shifter and the capture rate ε_{TIR} of the fiber:

$$p_{recapture} = Qy * \varepsilon_{TIR} \tag{6.6}$$

In this way, self-absorption not only brings about an effective increase in attenuation for all photons that are not recaptured, but also a change in the spectrum towards higher wavelengths. On the one hand due to the higher attenuation of the photons with shorter wavelengths and on the other hand due to the redistribution of the absorbed photons towards higher wavelengths. In order to check how strong this effect is, the emission spectrum of a oWl-fiber can be tested for a distance dependency.

6.4.2 Testing for Self-Absorption

To measure the emission spectrum, the WOM test stand can be used Fig. 5.7, whereby the measuring PMT is replaced by an integrating sphere [4] connected to a spectrometer [5] Fig. 6.15. The integrating sphere is used to collect the emitted light

[4] Data sheet: [@21]
[5] Data sheet: [@22]

of the fiber independent of the angle of the emitted photons, however since we only place the fiber inside the sphere we don´t have any coupling, increasing the effects of back reflection in the fiber.

Since the spectrometer is read out directly by the computer, the chopper with amplifier can not be used for background reduction. So a separate measurement without illumination of the rod is performed to remove the background. The rod itself is a $1\,\mathrm{m}$ long quartz rod with a diameter of $5\,\mathrm{mm}$ and coated with the WOM-paint over half its length.
In order to measure the effects of self-absorption we have to measure at the beginning of the paint layer. However, the WOM-test stand does not allow moving the LLG with the collimator that close to the sensors. So the rod was mounted with the uncoated side facing the sensor such that the beginning of the paint layer was reachable for the LLG. In the evaluation, the part that the light passes through the uncoated part of the sphere is neglected due to the good light transmission of the quartz [6].

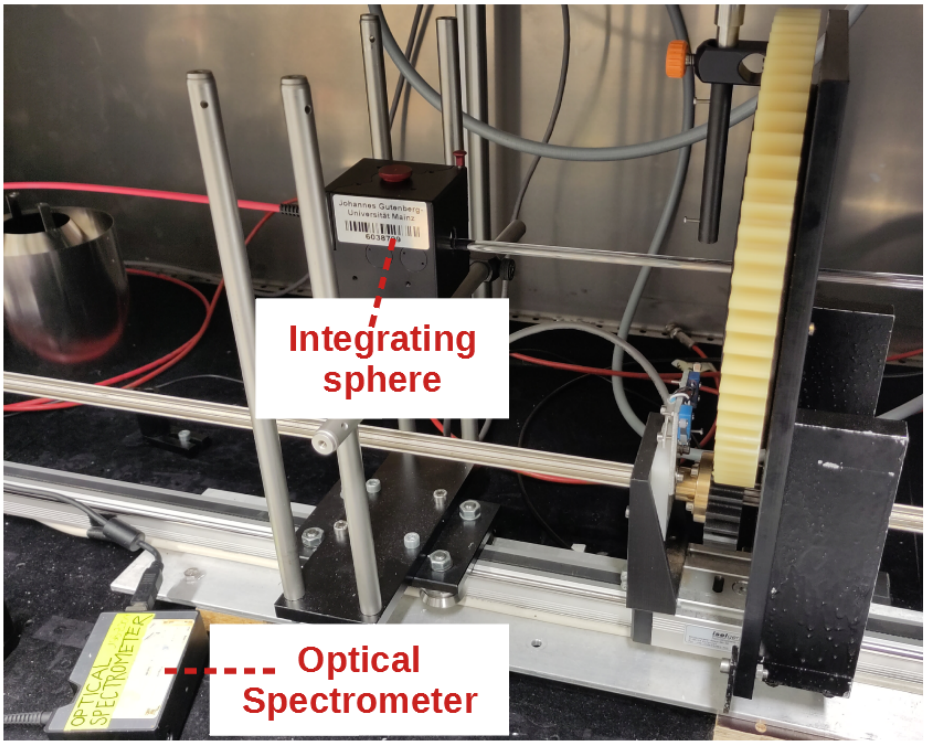

Fig. 6.15.: WOM test stand, but instead of the PMT an integrating sphere with a spectrometer is used.

[6] Transmission test of a used quartz rod can be found in the appendix Fig. A.15.

Results

The measured spectra in Fig. 6.16 shows a deviation from the reference spectrum of Bis-MSB. For example, the first peak at $400\,\mathrm{nm}$ can only be recognized in the first $10\,\mathrm{mm}$ until it disappears completely as seen in Fig. 6.17a. In addition, the peak at $425\,\mathrm{nm}$ is shifted towards higher wavelengths. The relative proportion of higher wavelengths increases for a greater distance from the spectrometer. The reason for this lies in the higher attenuation for photons with a wavelength below $425\,\mathrm{nm}$. The assumption that the relative increase is also due to an absolute increase due to the redistribution of the absorbed photons cannot be shown definitively. Thus, the intensity for the wavelengths above $425\,\mathrm{nm}$ increases in the first $50\,\mathrm{mm}$ which can be seen in Fig. 6.17b. However, if you also look at the integrated intensity of all wavelengths in Fig. 6.18a, it also increases in this range. The absolute increase therefore results from the measurement. One possibility is that the color layer is thinner in the first few mm and therefore less light is initially absorbed.

The only indication of the redistribution of the absorbed photons is a plateau formation at higher wavelengths, which does not match the later decrease Fig. 6.17b. These plateaus could indicate that losses due to attenuation within a wavelength are initially compensated by the addition of absorbed photons from other wavelengths.

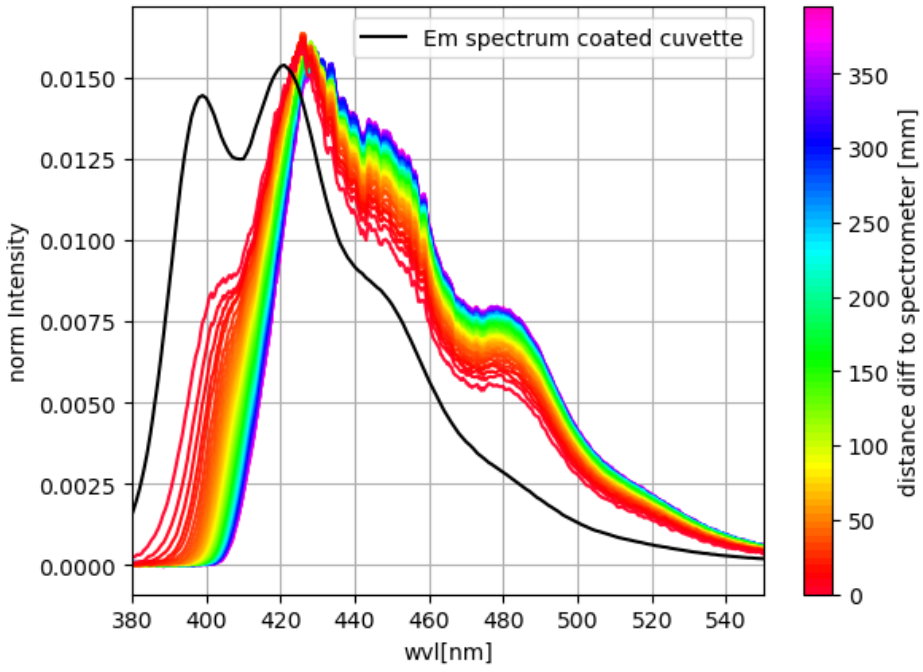

Fig. 6.16.: Measured emission spectrum of a coated $5\,\mathrm{mm}$ thick quartz rod for different illumination positions along the rod. The reference is taken by measuring the emission spectrum of a coated cuvette using the FS5

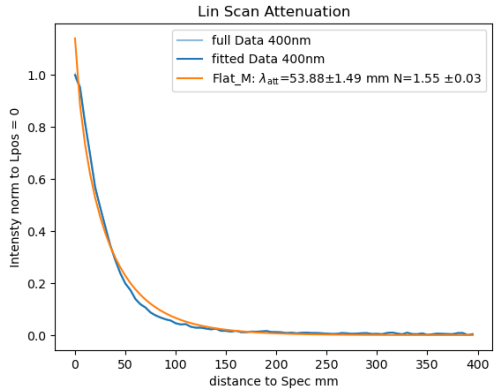

(a) Intensity at 400 nm.

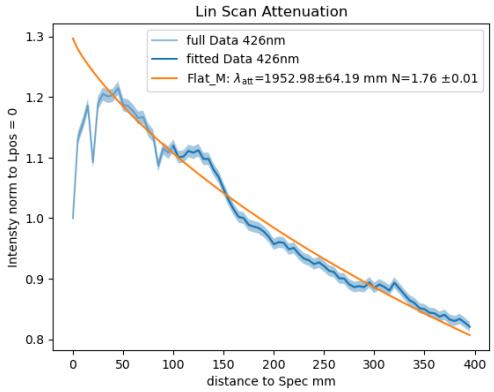

(b) Intensity at 426 nm.

Fig. 6.17.: Intensity at different wavelength, for each wavelength the effective attenuation is fitted with the flattened model Fig. A.10 and with the paint model Fig. A.11 for only attenuation in the paint

Fig. 6.18.

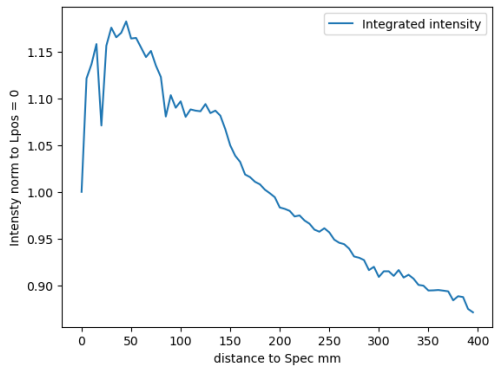

(a) Integrated intensity along the fiber showing an increase in intensity at the start

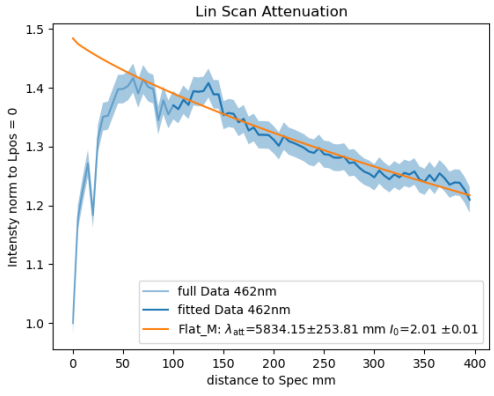

(b) Intensity at 462 nm

7 Self-Absorption Model

Now that we know that self-absorption plays an important role for the attenuation in the oWl fibers, we can create a model to describe the attenuation based on self-absorbance that also allows predictions for the oWl fibers and compare the predictions of the model with measured data.

7.1 A Self-Absorption based Model

To describe the fiber with self-absorption, the paint model (see subsection 5.2.1) must be adjusted. As the attenuation by the carrier and the matrix material differs from the self-absorption of the wavelength shifter, they have to be handled separately. The attenuation in the carrier and the matrix can be described by the paint model Eq. 5.7 by combining the to one attenuation length λ_{matter}. For the self-absorption, we calculate the effective absorption length λ_{self} with the paint model by setting the absorption in the carrier to 0 and also adding a wvl dependency Eq. 7.1.

$$\lambda_{self}(\varphi) \Rightarrow \lambda_{self}(\varphi, wvl) \tag{7.1}$$

But the bigger difference is the possibility of re-emission given by the Qy of the shifter. The reemitted photon gets a new direction $\theta_{new}, \varphi_{new}$ and is therefore lost if the TIR condition is not satisfied anymore.

Also it receives a new wavelength, since the wavelength shifter generally only shifts photons towards longer wavelengths due to energy conservation. The emission of a photon with a wavelength below the excitation wavelength is only possible if the photon hits an already exited state and is therefore suppressed [1]. The reemitted photons therefore are generally shifted away from the self-absorption region reducing the effect of self-absorption for higher orders of self-absorption. However for the model this effect was neglected due to the implementation effort. So for the

[1] A Measurement of an emission/excitation map in the self-absorption region can be found here Fig. A.18.

probability $p_{em}(wvl)$ of emitting a photon at a certain wavelength wvl we take the normalized emission spectrum $I_{em}(wvl)/I_{\text{total em}}$:

$$p_{em}(wvl) = I_{em}(wvl)/I_{\text{total, em}}. \tag{7.2}$$

Since the intensity at a certain wavelength depends on previous absorbed photons we describe the one-sided efficiency ε_{one} at a certain distance (z) using an recurrence relation. Therefore we split z into m sections $\Delta(z_n)_{n=0,..,m-1}$:

$$z = \sum_{n=0}^{m} \Delta z_n \tag{7.3}$$

The initial $(\varepsilon_{one})_0$ for each wavelength and photon direction is given by the TIR condition and the emission distribution :

$$(\varepsilon_{one})_0(wvl, \theta, \varphi) = \frac{1}{2\pi} H(\theta, \varphi)\ p_{em}(wvl) \tag{7.4}$$

To calculate the change to the next segment, $(\varepsilon_{one})n + 1(wvl, \theta, \varphi)$ we calculate the attenuation from the material $\lambda_{matter}(\varphi)$ and the reduction due to self-absorption $\lambda_{self}(wvl, \varphi)$. A portion of the total absorbed photons over all wavelengths (Total absorbed) Eq. 7.6, given by the emission spectrum ($p_{em}(wvl)$) and the capture rate ϵ_{cap}, is then added again.

$$\begin{aligned}
&(\varepsilon_{one})_{n+1}(wvl, \theta, \varphi) = \\
&(\varepsilon_{one})_n(wvl, \theta, \varphi)\ exp\left(-\frac{\Delta z_n}{\cos(\theta)}\left[\frac{1}{\lambda_{self}(wvl, \varphi)} + \frac{1}{\lambda_{matter}(\varphi)}\right]\right) \\
&+ \frac{\text{Total absorbed}}{4\pi} \cdot H(\theta, \varphi) \cdot \epsilon_{cap} \cdot p_{em}(wvl)\ exp\left(-\frac{\Delta z_n}{cos(\theta)\ \lambda_{matter}(\varphi)}\right)
\end{aligned} \tag{7.5}$$

$$\text{Total absorbed} = \int\int_{-\frac{\pi}{2}}^{0}\int_{-\frac{\pi}{2}}^{\frac{\pi}{2}} (\varepsilon_{one})_n(wvl, \theta, \varphi)\ \left[1 - exp\left(-\frac{\Delta z_n}{cos(\theta)\ \lambda_{self}(wvl, \varphi)}\right)\right]\ sin(\theta)\ d\varphi\ d\theta\ d(wvl) \tag{7.6}$$

The total $(\varepsilon_{one})_n$ is calculated by integrating over (θ, ϕ, wvl)

$$(\varepsilon_{one})_n = \int \int_{-\frac{\pi}{2}}^{0} \int_{-\frac{\pi}{2}}^{\frac{\pi}{2}} (\varepsilon_{one})_n(wvl, \theta, \varphi)\ sin(\theta)\ d\varphi\ d\theta\ d(wvl) \tag{7.7}$$

These formulas can now be used as the basis for a numerical simulation that covers the geometry, different attenuation wavelengths and self-absorption.

Alternatively it is also possible to simulate the intensity along the fiber by simulating single photons with a Monte-Carlo simulation. Such a simulation already exists for the WOM-Tube called WOMRat [23]. However, since this simulation was strongly optimized for the geometry of the WOM-Tube and the flattened model, it was not possible to add the self-absorption to this simulation in the course of this thesis.

7.1.1 Simulation

To calculate the expected intensity curve along the fiber we use the derived formula in section 7.1, the desired distance is divided into sections Δz. As the effect of self-absorption is highest close to the source, the sections here should be very small. This can be achieved by increasing the number of data points, but also results in an increase in computing time. In order to achieve a better resolution at the beginning with the same amount of data points, the data point density is chosen exponentially and the areas in between are interpolated as can be seen in Fig. 7.1a.
At the beginning of the simulation, the Heaviside function H(θ, φ) is calculated for all combinations of φ and θ. Then 2D distributions in θ, φ are created for the wavelengths in the emission spectrum.
With the initial distribution the number of self-absorption photons in the section Δd is calculated. The sum of the absorbed photons is then redistributed according to the emission spectrum and the capture rate. Finally, the regular attenuation by the substrate and matrix is calculated for the segment.
These steps are now carried out for all subsequent sections of the route until the entire distance has been simulated. After each section the expected total intensity I_n and its spectrum can be extracted. In order for the simulated intensity to match the measured data, the quantum efficiency spectrum must be applied to the simulated data. In our case, that of the measuring PMT Fig. 7.1b.

Fig. 7.1.

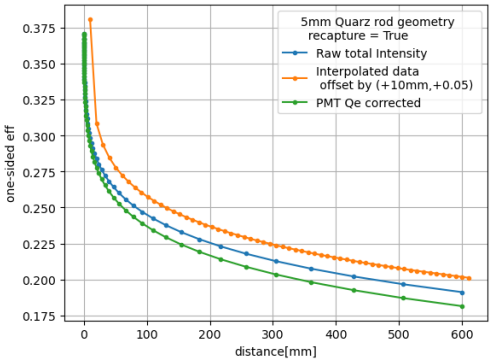

(a) Raw output of the simulation with exponential step size in blue. The interpolation of this data in orange(shifted for better visuals). For the green line the change in quantum efficiency of a PMT (right plot) was applied. The decrease is caused by the shift of the spectrum towards a less sensitive region in the QE

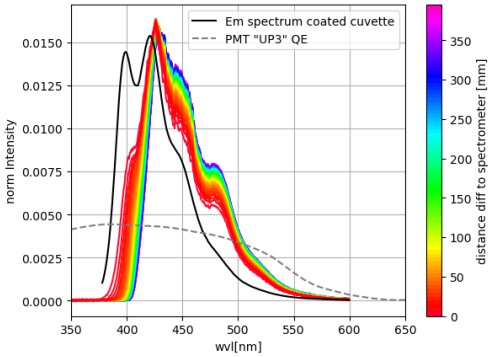

(b) Relative Change of the spectrum of a quartz fiber compared to the initial emission spectrum of a coated cuvette and the Quantum efficiency of PMT. The spectrum gets shifted towards higher wavelength where the QE of the PMT is lower, this leads to a decrease in measured Intensity simulated in the left plot.

7.1.2 Testing the Simulation

In order to compare the simulation with data, one can measure all parameters, insert them into the simulation and compare the result with the measurement. For this approach, not only the model must be correct, all parameters must also be determined independently. For the geometry, this is relatively simple, as the radius and length of the carrier can be measured using a measuring tape. The determination of the paint layer thickness can be calculated by the increase in mass Δm through the coating and the radius of the carrier R, with the coated length l_c. Eq. 7.8

$$d_{paint} = -R + \sqrt{R^2 + \frac{\Delta m}{\pi \, l_c \, \rho_{PEMA}}} \tag{7.8}$$

The attenuation length of the quartz rods can only be measured by measuring the light transmission through quartz rods of different lengths. In the case of the quartz rods for the oWl-fibers, a 1 meter long rod was cut into several smaller ones and the transmission measured Fig. A.15. The measured attenuation is so low that it can be assumed that the attenuation length is far greater than the length of the rod. However, it is not possible to make statements about the exact value, as the attenuation is in the order of magnitude of the measurement uncertainty.

To determine the absorption length of the shifter the UV-Vis subsection 6.3.2 can be used. However we ran into the same problem as the testing for clumping subsection 6.3.2, the range in which the UV-Vis can measure is limited by the emission of the shifter Fig. 6.7. This means that different concentrations have to be tested for their attenuation lengths. The resulting attenuation lengths are then converted to the same concentration (c), in this case the highest, which is $1170\,\mathrm{mg\,L^{-1}}$ using Beer´s Law Eq. 7.9. Giving Fig. 7.2b.

$$\lambda(c_1) = \lambda(c_2)\frac{c_2}{c_1} \tag{7.9}$$

The combined attenuation length saturates for the highest concentration at around $3\mathrm{m}$. This is an error caused by the minimum resolution of the UV-Vis. From Experience we know that even with the largest cuvette of 10 cm an attenuation length over $3\,\mathrm{m}$ is difficult to resolve. To obtain the complete spectrum, the data for the wavelengths above $440\,\mathrm{nm}$ are extrapolated with an exponential function.

For the measurement of the PEMA the best way would be a measurement of a coated PEMA slide, but even with a paint thickness of $100\,\mu\mathrm{m}$ an attenuation length over $4\,\mathrm{cm}$ would not be resolvable. Alternatively we measure the PEMA solved in toluene with the same ratio as in the paint Table 6.1, in the 10 cm cuvette giving a length of $1\,\mathrm{m}$ to $3\,\mathrm{m}$ Fig. 7.2a. However, this measurement also contains an inaccuracy, as the reference was measured with raw toluene resulting in a different concentration of toluene than is present in the paint.
The emission spectrum was measured with a coated slide in the FS5. Fig. 7.1b, as in subsection 6.3.3 this measurement is affected by self-absorption. As an alternative one could measure a low concentrated probe in the used solvent. But due to the now higher concentration of the solvent changing the also changing the spectrum Fig. A.2. The capture rate and thus the scaling of the intensity itself cannot be measured, only the theoretical value can be calculated from the refractive indices. Whereby we are also dependent on the manufacturer's specifications or literature references.

Especially for the attenuation lengths, the measurement of the parameter on their own is not sufficient to test the model due to all the possible inaccuracy during their measurement. However they still can be used as a reference and crosscheck for other methods.

Fig. 7.2.

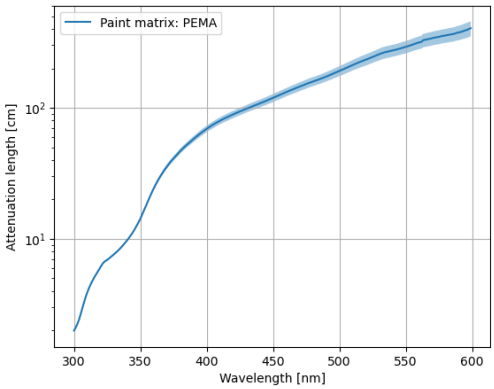

(a) Measured attenuation length of PEMA in toluene. For the important range over $425\,\mathrm{nm}$ the attenuation is around $2\,\mathrm{m}$

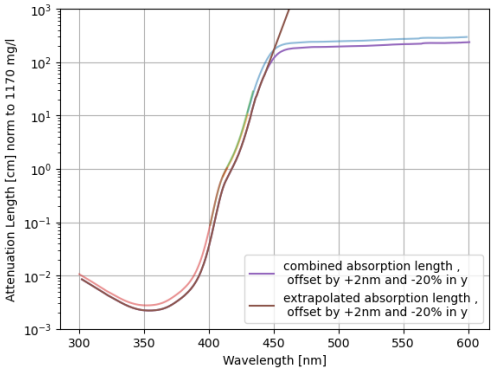

(b) Combined attenuation length spectrum of different concentrations of Bis-MSB tested in toluene Fig. A.13. Due to the saturation above $430\,\mathrm{nm}$ the spectrum is exponentially extrapolated.

Fitting

The other possibility to compare the data with the simulation is to fit the simulation to the measured data. However, one problem lies in the 3 used spectra. Fitting the complete emission and absorption spectra for each wavelength would result in a hundred of free parameters per spectrum making it unrealistic to fit the whole spectra. So in order to fit we have to make some assumptions for the spectra. The emission spectrum is set as a fixed parameter and the attenuation length in the matrix λ_{Matrix} is assumed to be constant over all wavelengths. For the shifters attenuation spectrum, the measured spectrum Fig. 7.2b is used and scaled by the scaling factor s_{Bis}. To reduce the fit parameters, the attenuation in the quartz carrier is set to 30 meters, as it has almost no influence on the total attenuation in the tested range of 25cm Fig. A.15.
The capture rate is also not fitted, instead we calculate the theoretical value from the refractive indices and again only fit a scaling factor N. Since the geometrical data are measurable they also wont be fitted only remaining three free parameter: s_{Bis},λ_{Matrix},N .

For the fit itself, the χ^2 Eq. 7.10 of the measured values O_i, their error σ_i and the values for the parameters E_i is calculated and minimized over the fit variables using a minimizer. Although we only have 3 parameters to fit, the attenuation in the matrix and the wavelength shifter cannot be determined independently due to their very similar effects. However, to obtain comparable results, we can use the measurements for the parameters subsection 7.1.2 as an orientation by modifying

the χ^2 with a prior. The prior receives the measured expected value y_m for a variable y and its uncertainty y_{err}, so if the minimizer searches outside the expected value of the variable, this get penalized by an increase in χ^2_P Eq. 7.11.

$$\chi^2 = \sum_i \frac{(O_i - C_i)^2}{\sigma_i^2} \tag{7.10}$$

$$\chi^2_P = \chi^2 + \frac{(y_m - y)^2}{y^2_{err}} \tag{7.11}$$

7.1.3 Comparing the Model to Measurements

For the comparison of the simulation with measured data, we can look at the 3 already shown measurements. First, the measurement of the WOM-Tube "Ultravision UQ3" Fig. 5.8, here we can fit the intensity for a large geometry. For a small geometry, we can use the measurements of the $6\,\mathrm{mm}$ thick quartz rod "Phoenix" Fig. 5.8. Finally, we can look at the change in the emission spectrum of a $5\,\mathrm{mm}$ thick quartz rod Fig. 6.16.

Attenuation

To compare the attenuation, we fit the self-absorption model to the data measured for the WOM-Tube. For the scaling factors of the intensity N and the attenuation length for the shifter s_{Bis}, we set a prior with an expected value of 1, which corresponds to the theoretical expectation of the photons to be captured and the measured attenuation length for Bis-MSB. The variance y_{err} for the two variables is set to 10% each. For the attenuation length of the matrix λ_{Matrix} a prior with an expected value of $3\,\mathrm{m}$ and an variance of $1\,\mathrm{m}$ is applied . The error was chosen to be so large to give the minimizer more room such that unconsidered effects, such as the surface quality, which would result in an increase in the attenuation can be represented in the matrix attenuation. In addition we compare the self-absorption model with the flattened Eq. 5.3 and the paint model Eq. 5.8 in their capability to fit the data Fig. 7.3. The fit parameters of the flattened model are the scaling factor N for the intensity, and the attenuation length in the fiberλ_{att}. The paint model is also scaled with the factor N and for the attenuation, only the attenuation length in the paint is fitted by setting the attenuation length for the carrier to $30\,\mathrm{m}$.

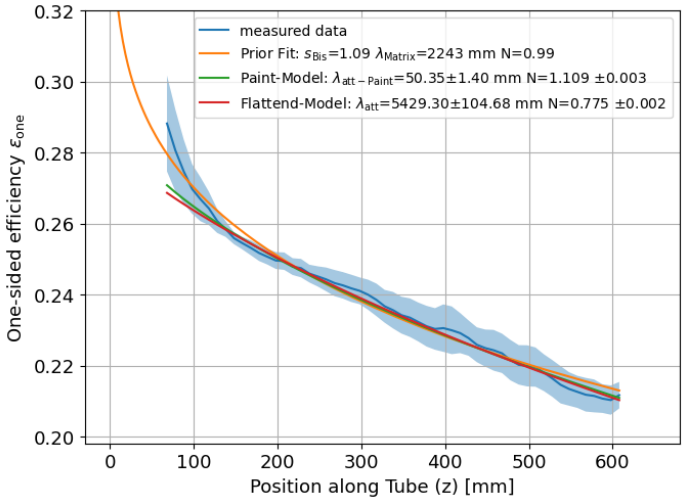

Fig. 7.3.: Fit of the flattened, paint and self-absorption Model to a measurement of the WOM-Tube "Ultravision".

Looking at the results Fig. 7.3 , one can say about all used models that their best fit lies within the error range of the data. However, all models show a systematic deviation for small distances which is the smallest for the self-absorption model. An indicator for the quality of a model is the scaling factor N. Here the flattened model must use a lower value than is expected 1 according to theory and the paint model a higher value. In contrast, the self-absorption model can describe the gap to the first data point better. In addition, the scaling factor for the absorption and matrix attenuation is also within the range of the measured data.

Now let's take a look at the measurement of the quartz rod Fig. 7.4.
If we first look at the progression, the flattened model again has problems reproducing the initial drop. Here, both the paint and the self-absorption model produce better results. Looking at the fitted parameters, no fit fulfills the expected value for N, but this deviation may come from the measurement, since the determination of the exact efficiency is not trivial and in contrast to that of the WOM-Tube not much analyzed subsection 5.3.2. The scaling factor for the shifter is still in the expected region, but the attenuation wavelength of the matrix falls into the cm range. So for the model to work, the light transmission in the matrix would have to be significantly worse for the smaller rod. Also when calculating the χ^2 for the measured parameter of (N=1,λ_{matter}=2000 mm,s_{Bis}=1) we get a value around 30000 for 71 data points highly excluding the model with these parameters.

The measured values for the fit parameters therefore only describe the geometry of the WOM-Tube and not that of the smaller rods. However, you can also test

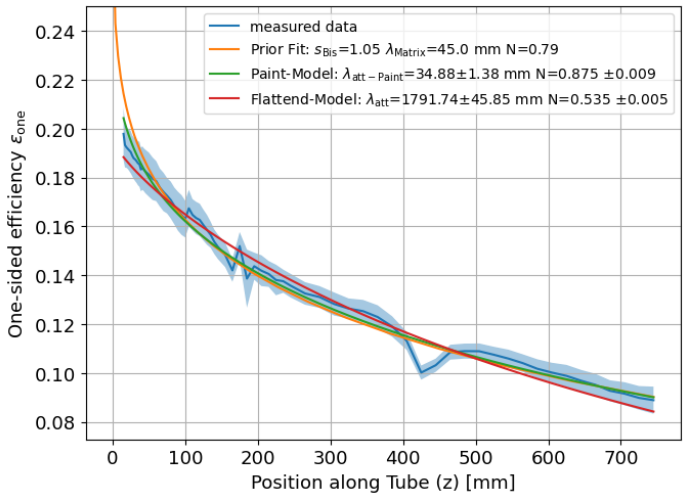

Fig. 7.4.: Fit of the flattened, paint and self-absorption Model to a measurement of an $6\,\mathrm{mm}$ diameter rod "Phoenix".

whether the values determined by the fit for the rods describe the WOM-Tube. To do this, we set the determined value for λ_{matrix} with $(50 \pm 30)\,\mathrm{mm}$ as a prior for a new fit of the WOM-Tubes data. To give the fit a little more flexibility here, the errors of N and s_{Bis} are increased to 20% Fig. 7.5. For the best fit we get for N=1 ,λ_{matter}=172 mm,s_{Bis}=1.24 and a $\chi^2 = 45$ for 55 data points. So the data can also be described with a general high attenuation in the paint, leaving no sensitivity for excluding a m

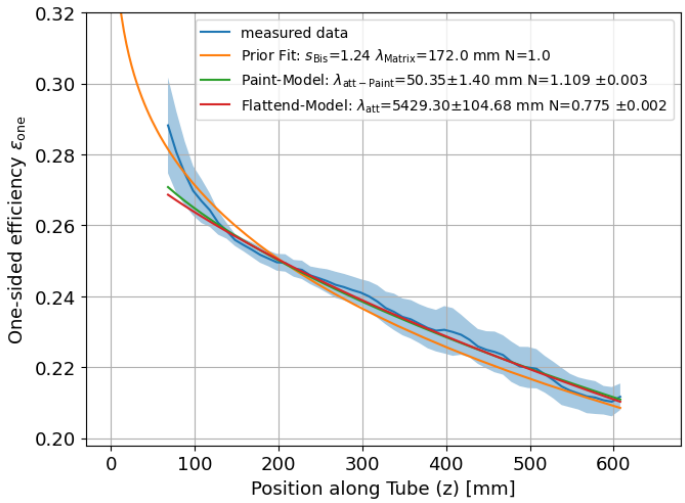

Fig. 7.5.: Fit of the flattened, paint and self-absorption Model to a measurement of the WOM-Tube "Ultravision" using the results of the fit of the quartz rod Fig. 7.4 as prior for the Fit

Spectrum

In addition, the simulation of the spectrum shape can also be compared with the measurement of the spectrometer. To do this, we can compare the normalized spectra of the $5\,\mathrm{mm}$ quartz rod with the prediction of the simulation. Unfortunately, the WOM-Tube is too big to be measured in the integrating sphere.

First, if we look at the measured spectrum and the prediction from the simulation Fig. 7.6, one can see that at the beginning the high attenuation of lower wavelengths below $400\,\mathrm{nm}$ are comparable suggesting that the wavelength dependent attenuation form the shifter works as predicted. But for higher wavelengths the measurement starts to differ from the prediction. While the measurement shows the second peak is mostly just reduced compared to other wavelengths and shifted slightly to higher wavelengths, in the simulation the second peak would vanish and a new peak would be crated, caused by the low attenuation Fig. 7.7 for the higher wavelengths. Also the measurement has a peak at around $480\,\mathrm{nm}$ which is not present in the simulation.

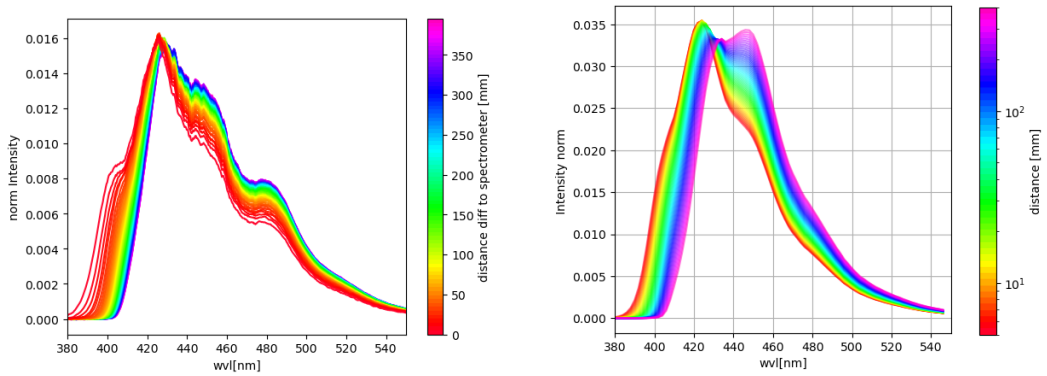

Fig. 7.6.: On the left the measured spectrum of a $5\,\mathrm{mm}$ quartz rod, on the right the simulation of the spectrum with the measured parameter from subsection 7.1.2 both starting at $5\,\mathrm{mm}$(Be aware of the different color scaling)

Now its not a surprise the spectra don´t match, since the fit of the attenuation length showed that the measured parameter don´t match the fitted. If we instead use the parameter determined by the fit of the $6\,\mathrm{mm}$ Fig. 7.4 rod with the higher matrix attenuation we observe a much better data-to-simulation agreement in the higher wavelength region. But still missing the $480\,\mathrm{nm}$ peak.

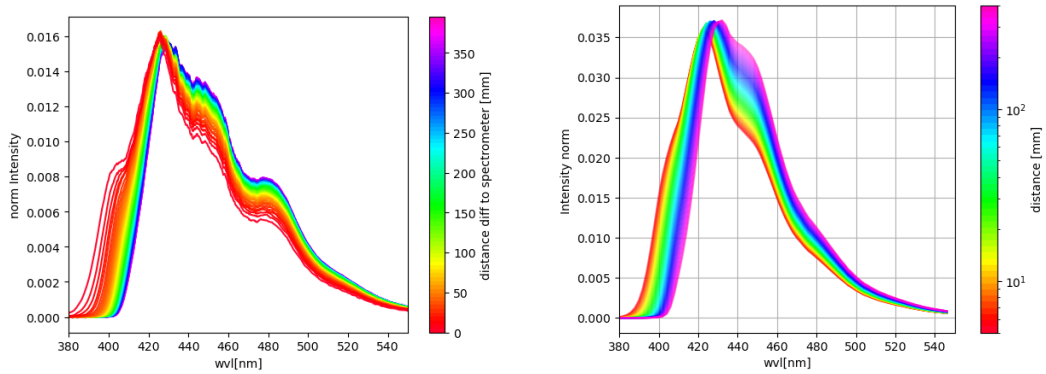

Fig. 7.7.: On the left the measured spectrum of a 5 mm quartz rod, on the right the simulation of the spectrum with the fitted parameter for the self-absorption model from Fig. 7.4 both starting at 5 mm(Be aware of the different color scaling)

7.1.4 Reasons for the Deviation

The self-absorption model manages to describe the attenuation in the WOM-Tube better than the other two models. When applied to the smaller rods, the shape can be reproduced, but the parameters determined for this differ from the measured and expected values. Thus, the attenuation for the smaller quartz rods increases significantly more than would be predicted by the model. We also see a significant difference in the shape of the spectra.
The reasons for the differences could be an incomplete or incorrect simulation, but it could also indicate problems in the production and measurement of the oWl-fibers.

Incomplete Model and Software Limitations

First of all, there are the same problems that occur with any numerical simulation, limited resolution and the possibility of edge effects, which can be reduced with a higher resolution and more computing time.
It is also possible that the fixed input parameters have errors. As small errors occur in the spectrum, such as a shift caused by measuring the liquid paint instead of the dried paint. These errors are amplified by the repeated application of self-absorption to the data in the simulation. Also this could led to shifts in the spectrum. However those errors can not explain the large differences for the attenuation length.
One point that could explain this and is the neglection of the difference in refractive indices for the paint and the substrate. For example, pure quartz glass has a refractive index of 1.47(at 425 nm) [@11] and the PEMA used 1.50 (at 425 nm) [@24] [2].

[2]Since no data was found for PEMA in the range, the value for PMMA was used which is very similar to PEMA

Therefore, refraction and total internal reflection can also occur in the transition from PEMA to quartz glass. As a result some of the photons can not leave the paint at all and are therefore more attenuated. Since the angle at which a trapped photon hits the inner radius is flatter than the outer radius, this effect is amplified especially for smaller geometries. This effect already has been simulated for the WOM-Tube where it was shown that this would have an effect on the attenuation [25]. So this may explaining the drastic decrease of the attenuation length for the smaller rods.

Hardware Challenges

It has been shown in the fits that the quartz rod can only be described for a high attenuation in the matrix material. Since the measurement of the WOM-Tube can be described for both high and low attenuation in the matrix, this could indicate that the attenuation in the paint layer after application is greater than the measurement of the liquid PEMA would suggest. Besides the increase of the relative paint thickness, the ratio of surface to volume increases for smaller geometries. So problems with the surface due to contamination or damage leading to a reduction in light transmission could explain the decrease for smaller geometries. However, looking at the the surface quality of the paint layer tested for test slides Fig. 6.3 do not give us any indication of general surface problem, also effects of the high concentrated Bis-MSB like clumping could be excluded subsection 6.3.2.

But in case of the small rods we do not have a measurement of the surface quality. And in case of the coating we ran into the problem, that the coating stand and its equipment is build for the WOM-Tube and not for small quartz rods. Thus, the positioning and fixing of the WOM-Tubes in the dip-coater is very stable, as the weight is attached to the bottom of the tube. In contrast is the weight of the rods attached at the top during coating, which means that the rod is not pulled out perfectly vertical. Another problem is the filling height of the paint vessel, as only a $50\,\mathrm{cm}$ deep bath was used to produce the WOM. In order to coat longer rods, the rod has to be coated in a two-step process, where you first coat half the length and then turn it around to coat the other half. During the second coating, however, the surface of the first coating is exposed to the solvent's vapors which damages the surface.Fig. 7.8 This effect can be reduced by applying the two coatings directly after each other so that the first side has no time to dry. However, the fact that the surface of both coated sides looks similar and measurements of half-coated rods have a similarly poor attenuation suggest this effect not to the main issue here.

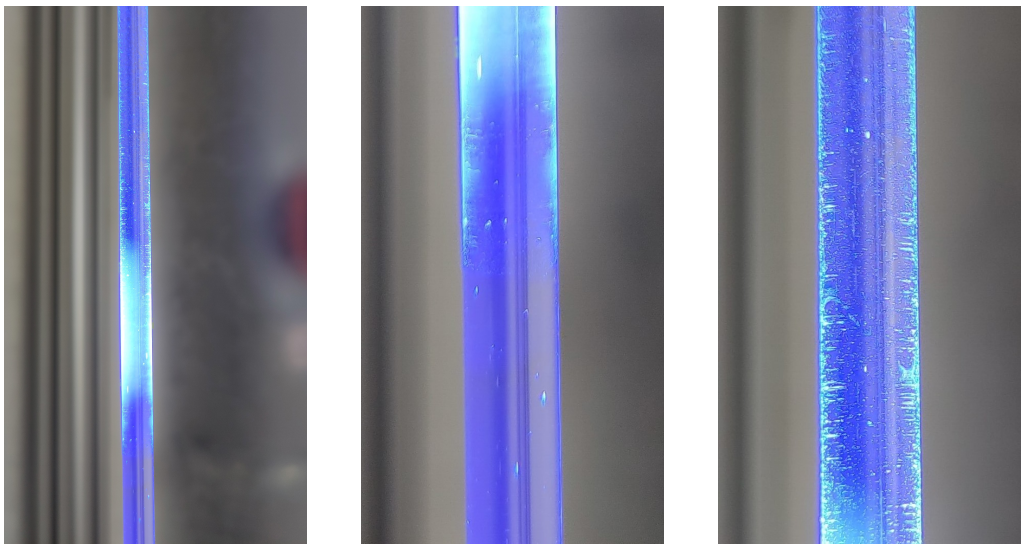

Fig. 7.8.: A double-sided coated oWl fibre. The sides were coated and dried one after the other. In the pictures on the left, the "new" paint layer is at the bottom of the picture and the "old" one at the top. The rod is illuminated with an UV lamp. The image in the middle shows the zoomed-in section below the illumination point and the one on the right shows the section above. If one compares these sections, the damage caused by the solvent on the first coating can be clearly seen in the numerous bright areas where the surface and light line are damaged.

Another possibility is that the surface can be damaged or contaminated afterwards. The accumulation of stains or dust can create scattering centers on the surface which destroy the light guidance at these points. The occurrence of stains may be resolved by cleaning, whereby the chemical resistance of the matrix must be taken into account. Also pressure marks in the PEMA during the handling would lead to a reduction of the light guidance, which could be reduced by using a harder material as a matrix.

Another possibility is the accumulation of dust. If you look at the materials used, they are all electrically non-conductive and therefore become statically charged during use, causing dust to be attracted.

In this way, dust can accumulate during the entire production process of cleaning, coating, storage and measurement of the rods. Especially accumulated dust during the first two points, is not possible to remove afterwards.

What also speaks for possible surface contamination is that the attenuation length for later measurements of the WOM-Tube has steadily decreased.

Conclusion and Outlook

8

This master thesis focuses on a new concept for wavelength-shifting fibers with high photon capture rates.
The first part outlines the strategy for achieving this improvement through the optimization of the absorption zone. Subsequently, this thesis investigates the resultant changes in timing and absorption parameters due to this optimization. Finally, the research presents a model designed to describe the characteristics of the newly developed fibers which is compared with measured data.

During this thesis we looked into the possibility to improve the capture rate of wavelength-shifting fibers. In commercially available fibers the wavelength shifter molecules are distributed isotropically in the fibers core. However, from a purely geometrical argument (see section 4.1), it is advantageous to situate the wavelength shifter molecules as close to the fibers surface as possible. The increased overall capture efficiency has been successfully shown in the WOM project[3] using large diameter hollow tubes and is now applied to small diameter fibers. The theoretical gain in TIR capture efficiency is a factor of 2 in the case of a quartz fiber with air as surrounding medium. For smaller differences in refractive index between the media, the factor is higher, we obtain a factor of 4 for the case of the same fiber in water.
It was investigated how the performance parameters timing, TIR capture efficiency and attenuation are affected when the carrier material is reduced to the order of mm. It was observed, that timing and TIR capture efficiency are not affected by scaling down the fiber. Measurements showed however, that the attenuation lengths of the produced fibers were around $2\,\mathrm{m}$, being smaller than for the WOM and commercially available fibers with approximately $3\,\mathrm{m}$. In the following, possible reasons for the lower attenuation length have been investigated in detail. A first ansatz for this reduction was the possibility of a higher amount of self-absorption due to the higher relative amount of paint thickness compared to the fiber diameter. Experimental investigations showed, that self-absorption does play a role in the lower part of the emission spectrum, while longer wavelengths are not affected which in turn means, that also the attenuation is not affected by self-absorption after long distances in the order of $1\,\mathrm{m}$.
Another possible reason for the lower attenuation length is the difference in refractive indices between WLS-paint and carrier material, which leads to trapping of a

number of photons inside the paint. It is also possible that the surface quality of the paint is worse, or has a higher impact on fibers than on the WOM. Surface quality measurements should be carried out in the future. The question whether a different attenuation in the paint layer compared to the carrier material could explain the lower attenuation is difficult to tackle. Here it is advised to enhance the current existing simulation of the fibers with the effects of self-absorption and a distinction between WLS-paint layer and carrier material in terms of attenuation.

In the case of a successful development of this technique with higher attenuation lengths it would be possible to bring the oWl-fibers to broad usage. The option to choose from a variety of wavelength shifters would allow accommodation of a large number of different situations.

Bibliography

[1]R. Abbasi, M. Ackermann, J. Adams, et al. “The IceCube data acquisition system: Signal capture, digitization, and timestamping”. In: *Nuclear Instruments and Methods in Physics Research Section A: Accelerators, Spectrometers, Detectors and Associated Equipment* 601.3 (2009), pp. 294–316 (cit. on p. 1).

[2]Discussion during group meeting with Prof. Dr. Michael Wurm ; Prof. Dr. Alfons Weber; Prof. Dr. Sebastian Böser (cit. on pp. 1, 9).

[3]Benjamin Bastian-Querner, Lucas S. Binn, Sebastian Böser, et al. *The Wavelength-shifting Optical Module*. 2022. arXiv: 2112.12258 [astro-ph.IM] (cit. on pp. 1, 8, 16, 19–21, 24, 32, 35, 63).

[4]Wolfgang Demtröder. *Experimentalphysik 2 , Elektrizität und Optik*. Springer - Verlag, 2017 (cit. on p. 3).

[6]Glenn F Knoll. *Radiation detection and measurement*. John Wiley & Sons, 2010 (cit. on p. 4).

[8]W. Bugg, Yu. Efremenko, and S. Vasilyev. “Large plastic scintillator panels with WLS fiber readout: Optimization of components”. In: *Nuclear Instruments and Methods in Physics Research Section A: Accelerators, Spectrometers, Detectors and Associated Equipment* 758 (Sept. 2014), pp. 91–96 (cit. on p. 9).

[10]Aya Ishihara. *The IceCube Upgrade – Design and Science Goals*. 2019. arXiv: 1908.09441 [astro-ph.HE] (cit. on p. 15).

[13]John Rack-Helleis. “Efficiency Determination of the Wavelength-shifting Optical Module (WOM)”. MA thesis. Johannes Gutenberg University Mainz, 2019 (cit. on pp. 29, 32).

[14]John Rack-Helleis. “(working title)The wavelength-shifting optical module for the IceCube Upgrade”. not yet published. PhD thesis. Johannes Gutenberg University Mainz, 2024 (cit. on p. 29).

[16]Dustin Hebecker. “Development of a single photon detector using wavelength-shifting and light-guiding technology”. PhD thesis. Humboldt-Universität zu Berlin, Mathematisch-Naturwissenschaftliche Fakultät, 2021 (cit. on p. 32).

[17]Jonas Hümmerich. “Optisch aktive wellenlängenschiebende Beschichtungen”. Bachelor’s Thesis. Johannes Gutenberg University Mainz, 2022 (cit. on p. 34).

[18]Conversations with Dr. Anastasia Mpoukouvalas and John Rack-Helleis about Clumping (cit. on p. 34).

[23]Florian Thomas. “Light propagation simulation for the Wavelength-shifting Optical Module on CUDA GPUs”. MA thesis. Johannes Gutenberg University Mainz, 2019 (cit. on p. 51).

[25]Moritz Robin Strauß. “Detaillierte Modellierung von Absorption im Wellenlängenschiebenden Optischen Modul”. Bachelor’s Thesis. Johannes Gutenberg University Mainz, 2023 (cit. on p. 60).

[26]Marie Wandel. “Attenuation in silica-based optical fibers”. PhD thesis. Technical University of Denmark and at OFS Denmark, 2005 (cit. on p. 69).

Webpages

[@5]Jfmelero (adapted by Gavin R Putland). *Plaques of Lambda Phages on E. coli XL1-Blue MRF*. 2019. URL: https://commons.wikimedia.org/wiki/File:ReflexionTotal.svg (visited on Dec. 18, 2023) (cit. on p. 4).

[@7]*Jablonski diagram of absorbance, non-radiative decay, and fluorescence.* 2021. URL: https://en.wikipedia.org/wiki/Fluorescence#/media/File:Jablonski_Diagram_of_Fluorescence_Only-en.svg (visited on Jan. 6, 2024) (cit. on p. 5).

[@9]Kuraray. *Plastic Scintillating Fibers*. URL: https://www.kuraray.com/uploads/5a717515df6f5/PR0150_psf01.pdf (visited on Nov. 18, 2023) (cit. on pp. 11, 12, 30).

[@11]*Arosa and de la Fuente 2020: n 0.26–1.7 µm*. URL: https://refractiveindex.info/?shelf=main&book=SiO2&page=Arosa (visited on Dec. 18, 2023) (cit. on pp. 18, 59).

[@12]Heraeus. 2024. URL: https://www.heraeus-conamic.com/de/brands/hsq#hsq_downloads (visited on Jan. 3, 2024) (cit. on p. 27).

[@15]HAMAMATSU. 2003. URL: https://user-web.icecube.wisc.edu/~kitamura/NK/PMT/031112%20R7081-02%20data%20sheet.pdf (visited on Jan. 9, 2024) (cit. on p. 32).

[@19]Perkin Elmer. *LAMBDA 650/850/950*. 2004. URL: https://cmdis.rpi.edu/sites/default/files/UVVis-PerkinElmer-Lambda950-HardwareGuide.pdf (visited on Nov. 21, 2013) (cit. on pp. 36, 37).

[@20]Edinburgh Instruments. *Edinburgh Instruments Website*. 2023. URL: https://www.edinst.com/de/products/fs5-spectrofluorometer/ (visited on Nov. 25, 2023) (cit. on pp. 41, 76).

[@21]Thorlabs. 2023. URL: https://www.thorlabs.com/drawings/cd0cc689d41fb27c-9A0F3803-AC56-ECED-003B6AE3C3C9925F/2P3_M-SpecSheet.pdf (visited on Jan. 6, 2024) (cit. on p. 44).

[@22]Ocean Optics. URL: https://www.oceaninsight.com/globalassets/catalog-blocks-and-images/manuals--instruction-ocean-optics/spectrometer/usb2000-operating-instructions1.pdf (visited on Jan. 6, 2024) (cit. on p. 44).

[@24]*Arosa and de la Fuente 2020: n 0.26–1.7 µm*. URL: https://refractiveindex.info/?shelf=organic&book=poly%28methyl_methacrylate%29&page=Zhang-Tomson (visited on Dec. 28, 2023) (cit. on p. 59).

Appendix

A

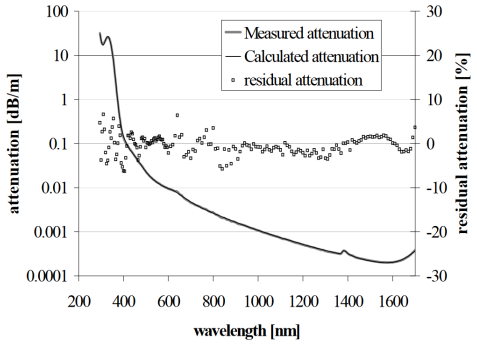

Fig. A.1.: Attenuation of a silica based fiber. Taken from [26]

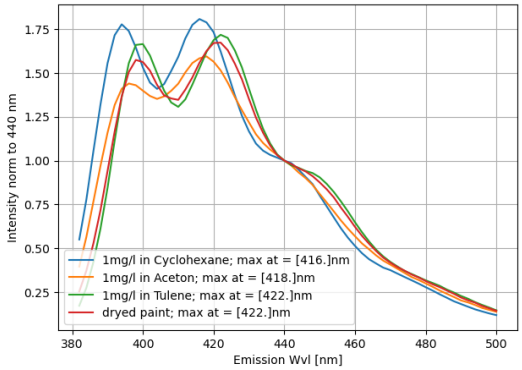

Fig. A.2.: Comparison of the emission spectrum of Bis-MSB in different Solvents. For toluene based probes(also dried Paint) the emission peaks is slightly shifted towards higher wavelengths.

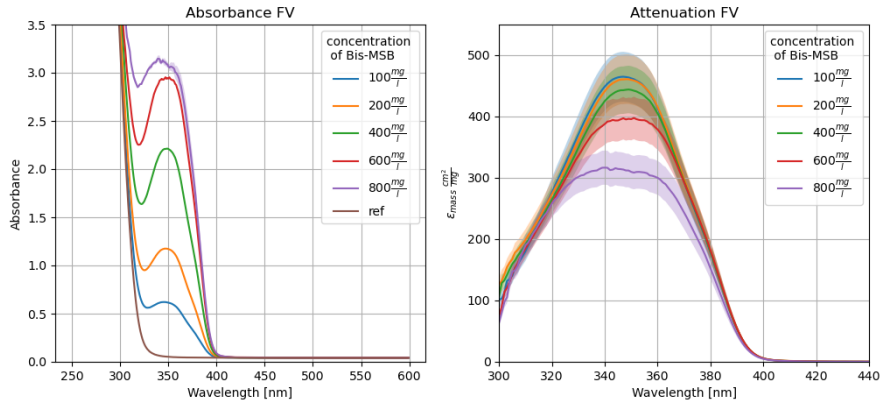

Fig. A.3.: Absorbance and calculated mass extinction for the F-Cuvette filled with aceton

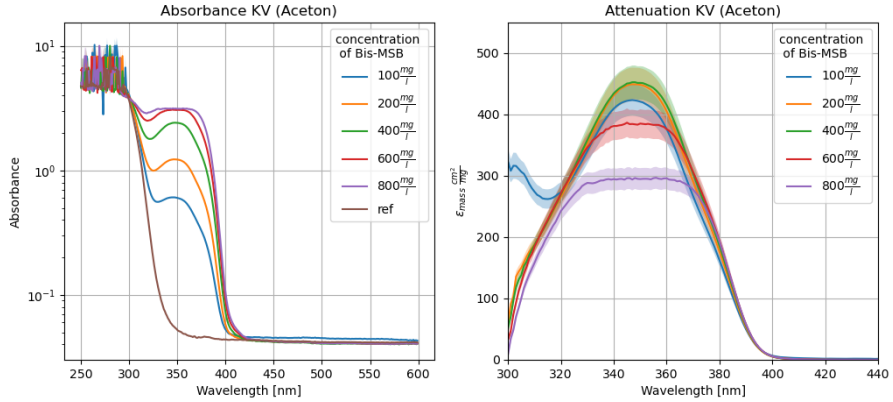

Fig. A.4.: Absorbance and calculated mass extinction for the K-Cuvette filled with aceton

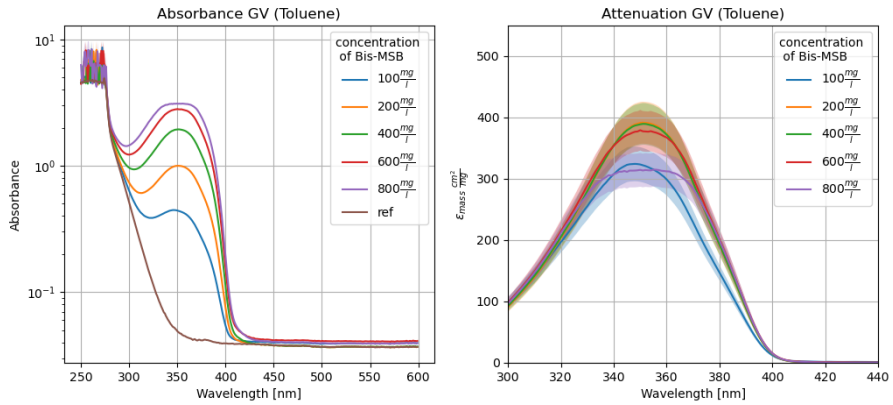

Fig. A.5.: Absorbance and calculated mass extinction for the G-Cuvette filled with toluene

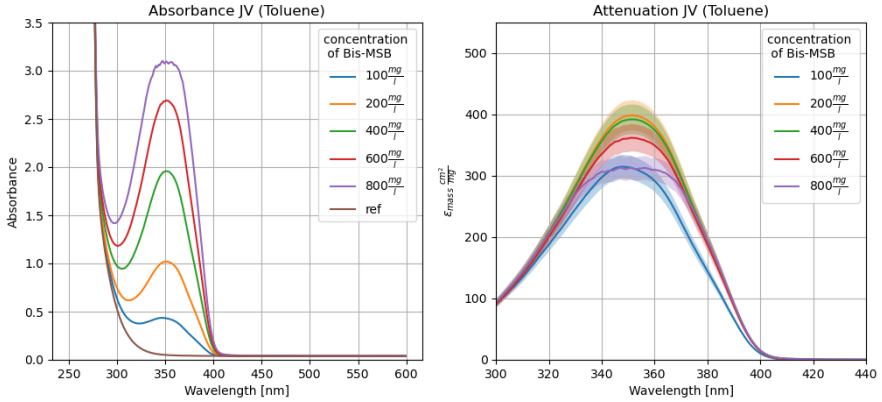

Fig. A.6.: Absorbance and calculated mass extinction for the G-Cuvette filled with toluene

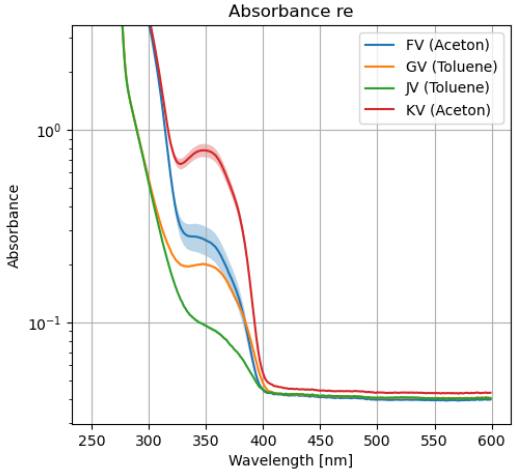

Fig. A.7.: Absorbance of the cleaned cuvettes after all samples were measured, one can see that even after cleaning remnants of Bis stayed in the cuvette

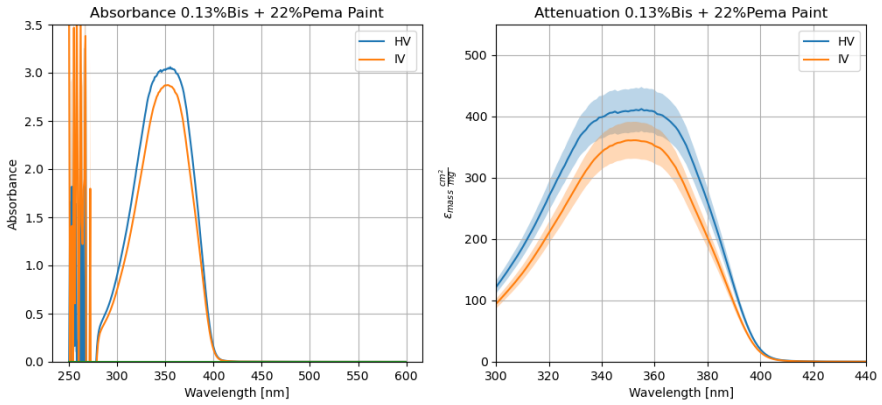

Fig. A.8.: Absorbance and calculated mass extinction for the H,I-Cuvette filled with the liquid Paint filled with 0.13 mass% of Bis-MSB and 22 mass% of PEMA in toluene

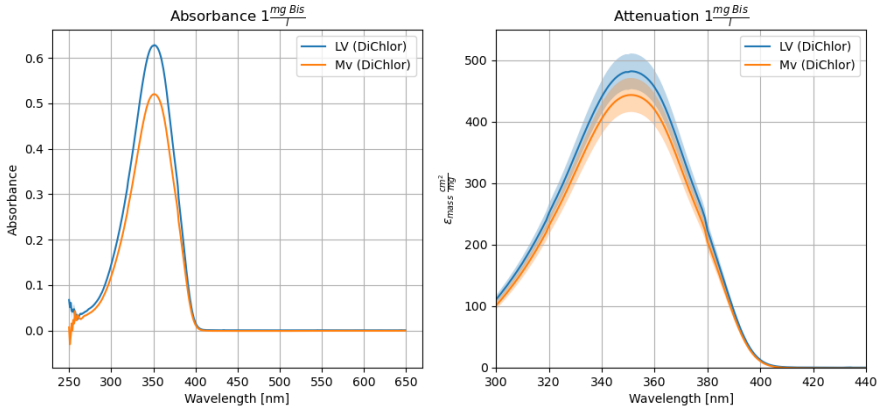

Fig. A.9.: Absorbance and calculated mass extinction for the H,I-Cuvette filled with dichlormetane

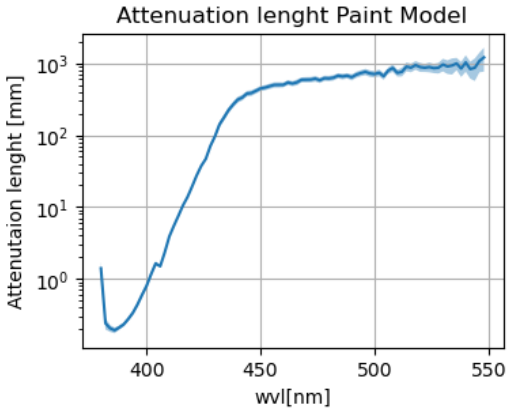

Fig. A.10.: Fitted attenuation length using the flattened model of the measurement of the emission spectrum Fig. 6.16. The starting point of the fit was increases for higher wavelength to reduce the impact of self-absorption and the systematic increase in absolute intensity.

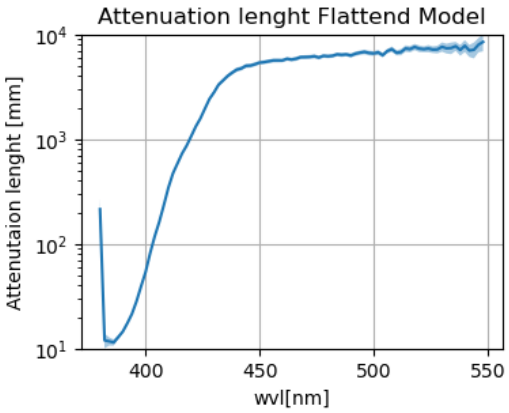

Fig. A.11.: Fitted attenuation of the paint attenuation length using the paint model of the measurement of the emission spectrum Fig. 6.16. The starting point of the fit was increases for higher wavelength to reduce the impact of self-absorption and the systematic increase in absolute intensity.

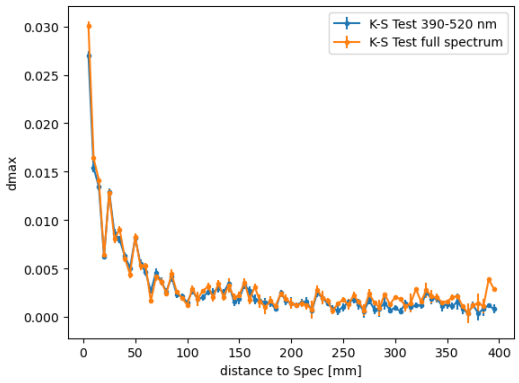

Fig. A.12.: Max difference of the spectrum to the next point on the z position.

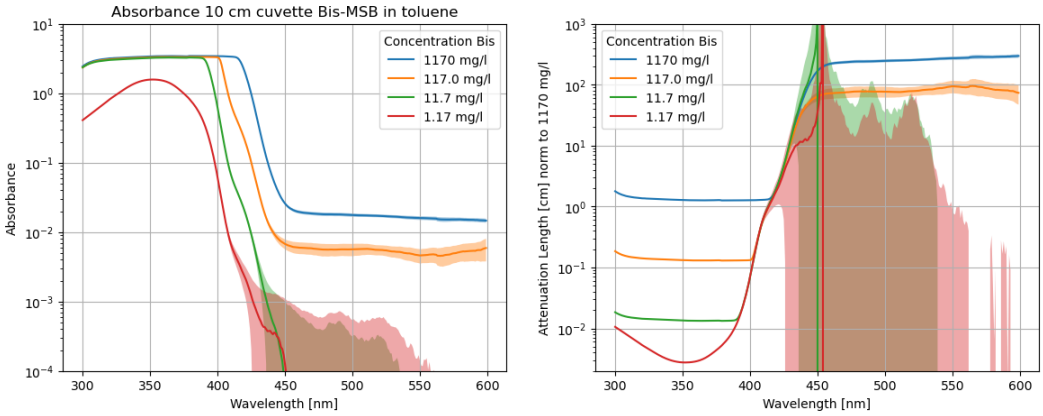

Fig. A.13.: on the left: Baseline corrected Absorbance for different Concentrations of Bis MSB. on the right the calculated Attenuation normalised to 1170 mg/l

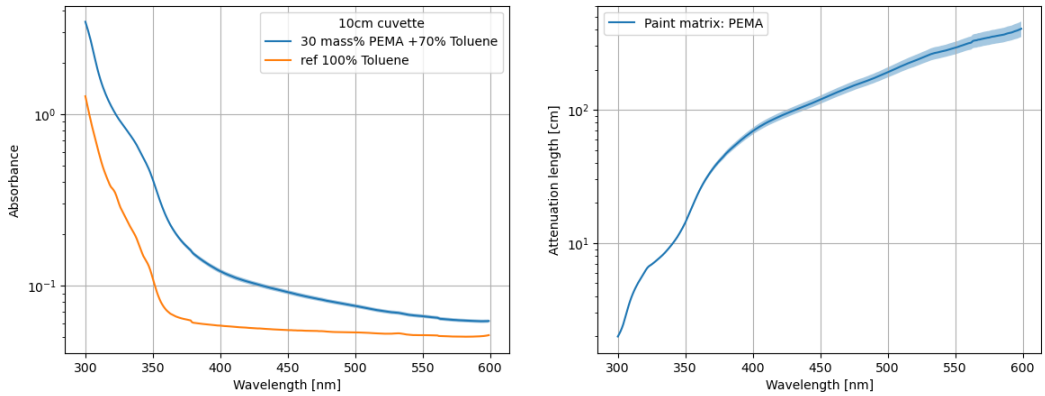

Fig. A.14.: Absorbance and Attenuation Length of PEMA solved in toluol

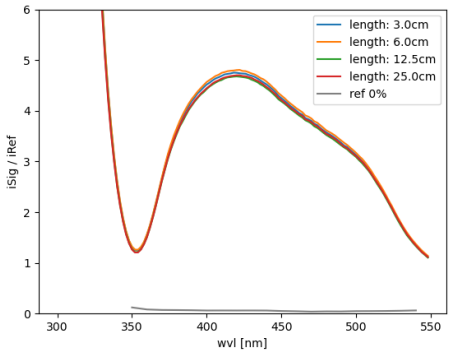

Fig. A.15.: Transmissions Measurement of one 6mm quartz rod divided in smaller rods

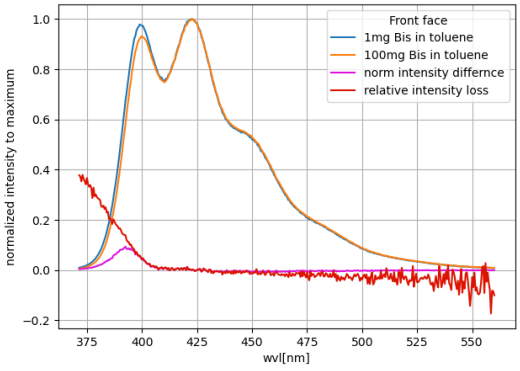

Fig. A.16.: Change of the emission spectrum for different concentration of Bis-MSB in toluene. Measured using the front face sample holder of the FS5 subsection 6.3.3. Due to the low concentration of 1 mg / l in the sample, the effects of self-absorption on the spectrum can be neglected.

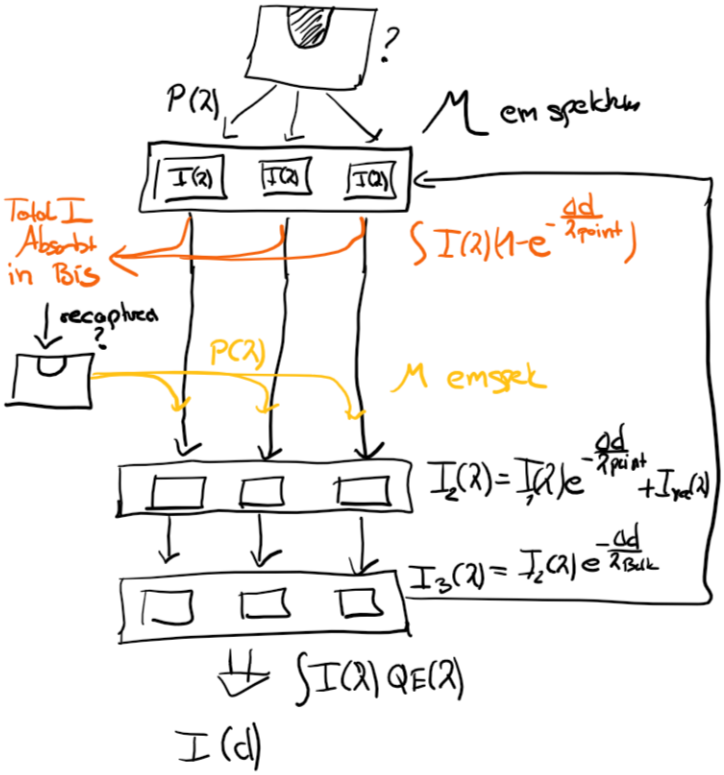

Fig. A.17.: Flow Chart of the Simulation

Emission Spectrum of the Self-Absorption

Usually the photons can only be re-emitted with the same or a lower energy. However, it is also possible that the thermal movement of the molecules can excite the photon to a state of higher energy, and thus they can also have a higher energy during re-emission. The probability is therefore dependent on the temperature. This effect was be measured with the FS5[@20] by exciting and measuring the shifter with light from the range of its emission spectrum. In doing so, it can be seen that the spectrum does not change for a higher emission to excitation wavelength. However, lower emission wavelengths than the excitation wavelength are suppressed the higher the excitation wavelength Fig. A.18.

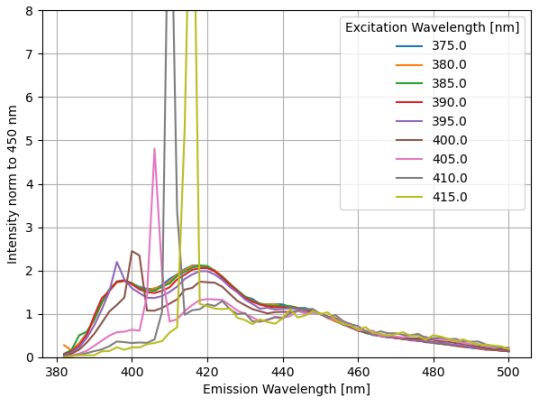

Fig. A.18.: Emission spectrum of Bis-MSB in cyclohexane for different excitation wavelengths [1]. The strong reduction of emissions below the excitation wavelength is clearly visible. The peaks at which the excitation wavelength is equal to the emission wave are due to scattering of the excitation light.

Declaration

I hereby declare that I have written the present thesis independently and without use of other than the indicated means. I also declare that to the best of my knowledge all passages taken from published and unpublished sources have been referenced. The paper has not been submitted for evaluation to any other examining authority nor has it been published in any form whatsoever.

Mainz, 10.01.2024

Bastian Keßler